Examenarsbete

TVVR 14/5003

In search for interannual and interdecadal relations between climate variability and continental freshwater discharge to the Mediterranean Sea

Author: Guido Sabatini

Supervisor: **Professor Cintia Bertacchi Uvo**

Thesis opponent: **Rebecka Jenryd and Rebecka Karlsson**

Examiner: **Professor Magnus Persson**

Lunds Universitet

Master of Science programme in Water Resources

Department of Building and Environmental Technology

10/03/2014

Acknowledgements

I would like to express my sincere gratefulness to the all fantastic staff (Professors, officers, coordinators) that I have met here at Lund University. Thank you for having let me be part of this highly qualified Institution in one of the most welcoming Countries I have ever been.

A particular thanks goes to Professor Cintia Bertacchi Uvo for all the valuable support and heartfelt help that have been provided throughout the thesis work.

Thanks also to Rebecka Jenryd and Professor Magnus Persson for taking the time to be, respectively, my thesis opponent and examinator.

Grazie a Voi, e a Te, che mi avete sostenuto in ogni modo durante questi due anni, che mi siete mancati cosí tanto e che oggi siete con me.
Grazie ad Ettore e ai suoi Genitori perché insieme siete felici e mi fate ben sperare.

Abstract

Variability of atmospheric circulation is considered one of the most important factors causing interannual and interdecadal variability of freshwater amount that is discharged from the continents. Here it is presented an analysis of the relations between the discharge variability of five major rivers in the Mediterranean basin (i.e. Adige, Arno Ebro, Po and Rhone) responsible for the 70% of total freshwater input into the Mediterranean Sea, and the variability of four atmospheric circulation patterns: East Atlantic (EA), North Atlantic Oscillation (NAO), Scandinavia (SCA) and Pacific Decadal Oscillation (PDO).

River discharge measurement data, collected from the relevant Authorities and Hydrological Institutes, cover periods between 52 and 91 years. The wavelet method is used to analyze, singularly, the time series of non-stationary events. Cross Wavelet Transforms (XWT) are constructed to highlight common wavelet power and relative phase in the time-frequency domain of the analyzed time series. Monte Carlo method is used to assess the significance level of the results.

Results show the influence of teleconnections patterns on rivers' discharge in the Mediterranean basin. The NAO, SCA and PDO teleconnections patterns have the highest impact on the freshwater flow variability in the Mediterranean Sea. The NAO shows periodically its anti-phase behavior with most of the analyzed discharge time series in the ≈2 and ≈16 year periods; the Scandinavia teleconnections patterns is in-phase with discharge time series in the ≈2 and ≈8 year periods; the XWTs involving PDO show relevant common power and in-phase behavior in correspondence of the 20-30 year period, in accordance to the nature of this pattern which in characterized by low frequency variations. Results involving the EA teleconnection pattern show are conflicting with other relevant studies since positive phases of the EA do not lead, as expected, to the observation of below-average river discharge precipitation across southern Europe.

Although this type of evaluation is purely qualitative and does not allow to quantify the direct impact of teleconnection patterns on river discharges, these potential relations can be useful to predict climatological events occurring over the Mediterranean basin and the results of this study could constitute a strong basis to achieve a first prediction about future changings in the availability of freshwater resources in Europe.

Acronyms

Teleconnection patterns	
EA	East Atlantic
NAO	North Atlantic Oscillation
PDO	Pacific Decadal Oscillation
SCA	Scandinavia

Wavelet analysis	
CWT	Continuous Wavelet Transform
DWT	Discrete Wavelet Transform
XWT	Cross Wavelet Transform

Table of Contents

1. Introduction

The variability in atmospheric circulation conditions plays a key role in determining spatial distribution changes of precipitation, temperature and other climatological elements (Martìn et al., 2003). As a consequence, atmospheric circulation variability at different space and time scales has an influence on annual and decadal variability of freshwater fluxes that flow from the continents to oceans and seas (Bouwer et al., 2008). The term "teleconnection pattern" refers to a recurring and persistent, large-scale pattern of pressure and circulation anomalies that extent over vast geographical areas. The investigation on specific periodicities of the climate signals, over which multiple terrestrial phenomena can be linked with each other, is of particular interest in teleconnection research. Although patterns typically last for several weeks to several months, they can sometimes be prominent for several consecutive years, thus reflecting an important part of both the interannual and interdecadal variability of the atmospheric circulation, having also an impact on river discharge (CPC, 2014).

The understanding of the nature of teleconnections in terms of amplitude, phase and periodicity is decisive for the analysis of regional climate variability and change. The possibility of relating a certain regional climate to specific circulation patterns could lead to a significant improvement in what concern seasonal estimation (Lidén et al., 2012). Such seasonal and longer time-scale estimations could have direct effect on human activities an lives, as they are often associated with droughts, floods, heat waves and cold waves and other changes that can deeply affect sectors such as agriculture, water supply and fisheries, and can modulate air quality, fire risk, energy demand and human health (IPCC, 2007).

As teleconnection patterns reflect large-scale changes in the atmospheric climate and influence temperature, rainfall, storm tracks and jet stream intensity over vast areas, in this contribution we investigate the discharge time series of five rivers in the Mediterranean area relating them to four climate indices.

1.2. Objective

The objective of this study is to individuate periodical relations between long-term oscillations in river discharge in the Mediterranean basin and single teleconnection patterns (i.e. EA, NAO, PDO and SCA).
However, such relations only reflect qualitative expectations in terms of increase or decrease in river discharge under specific teleconnection patterns conditions and do not allow in any case to quantify the variation of freshwater that is discharged into the Mediterranean Sea.

2. Description of the study area: the Mediterranean Basin

River discharge is one of the five components of the Mediterranean Sea water budget. Indeed, along with the net water inflow from Atlantic Ocean through the Strait of Gibraltar, the one from the Black Sea through the Dardanelles Strait, evaporation (E) and precipitation (P), river discharge (R) represents one of the contributions to this water budget. Although river annual mean discharge in the Mediterranean basin constitutes less than 20% of the atmospheric water budget (i.e. the difference between evaporation and precipitation), river discharge and precipitation are the only freshwater inputs into the basin, and during spring the two basin-integrated components E − P and R are fairly comparable. Moreover, for coastal regions where the major rivers discharge, freshwater input from rivers is quite significant and discharge variability can play a key role in modulating the characteristics of the Mediterranean environment (Struglia et al., 2004).

The variability of Mediterranean river discharge is strongly based on the atmospheric water budget as well as on the geographical characteristics of the Mediterranean catchment. Geographically the Mediterranean catchment is extremely heterogeneous, extending from the source of the Nile River, approximately at the equator, to the source of the Rhone River around the 48°N. It consists of great valleys, such as the Nile and the Rhone valleys or the Po plain, high mountains, such as the Alps, where most of winter precipitation is in form of snow, and mountains, such as the Atlas in northeastern Africa and the Taurus in Turkey, that can capture moisture by means of orographic effects from eastward-propagating mid-latitude cyclones generated in the North Atlantic Ocean and in the eastern Mediterranean Sea (Struglia et al., 2004).

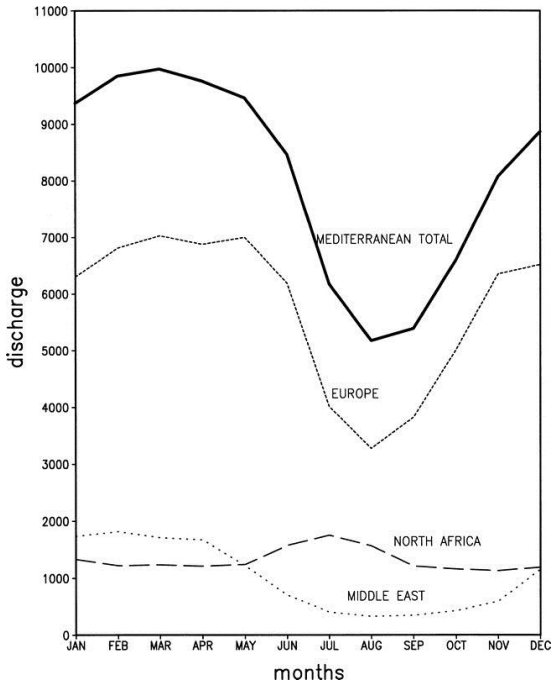

Figure 1: Seasonal cycle of total discharge into the Mediterranean Sea and its decomposition by continent of origin (Struglia et al., 2004)

The continental river discharge into the Mediterranean Sea is mainly associated with Rhone, Po, and Nile rivers that discharge, respectively, about 1700, 1500, and 1200 m3 s−1. Secondary, but still relevant contributions, are from Ebro, Arno and rivers on the eastern Adriatic coast (e.g. Adige). Very little is contributed by North African rivers, other than the Nile (Struglia et al., 2004).

Fig. 1 shows how discharge is greatest from late fall to spring periods, with a peak flow of about 10×10^3 m^3 s^{-1} occurring in late winter. Minimum discharge is in late summer (about 5×10^3 m^3 s^{-1}). Climatological annual mean Mediterranean discharge has been evaluated around 8.1×10^3 m^3 s^{-1}. Struglia et al., 2004, estimates that Mediterranean discharge does not exceed 10.4×10^3 m^3 s^{-1}, taking into account possible underestimations of the previous given value. Many other studies have estimated different values that are unfortunately not easily comparable because of the differences in methods and data used.

Fig. 1 also displays different contributions to the total discharge by specifying the continent of origin. European discharge appears as the main contributor, clearly determining the time curve of the whole Mediterranean seasonal cycle. This includes discharge from the Rhone, Po, and Ebro that are the three

major European rivers, whose annual mean discharge is estimated around 5.7 × 10^3 m^3 s^{-1} (Struglia et al., 2004), around the 76% of the total annual mean discharge. The seasonal cycle has its minimum of about 3 × 10^3 m^3 s^{-1} in mid-late summer and its maximum from fall to spring of about 7 × 10^3 m^3 s^{-1} (Struglia et al., 2004).

The Middle Eastern seasonal cycle has an analogous time behavior, with a very broad minimum in summer, a broad maximum in winter, but a much lower annual mean discharge. North African discharge is mainly due to the Nile River: given the fact that Blue Nile, the largest tributary of the Nile, drains the Ethiopian Plateau where intense precipitation falls during the summer months, the African contribution has its peak (about 1.7 × 10^3 m^3 s^{-1}), during that period.

Figure 2: The Mediterranean Basin and rivers 'outlet (Weather Almanac, 2014)

2.1. Adige river basin and its regulatory framework

The Adige is the second longest Italian river, and drains an area of around 12,100 km² located in the North - East of Italy, in the Trentino Alto-Adige and Veneto Regions. The Alpine upper part of the river covers most of its drainage basin as in downstream areas the river receives no tributaries (see Figure 3). The Adige headwaters are mainly fed by snowmelt and rain and by 185 glaciers with a total glacial surface of about 200 km^2. Before reaching the outlet in the Adriatic Sea, Adige river covers a length if 409 km (Bruno et al., 2014).

Figure 3: Adige river basin (Autorità di Bacino del Fiume Adige, 2014).

Similarly to large Alpine rivers, the Adige has been greatly altered during the last century. In the 1920s, the development of large water uses for hydropower generation and irrigation framework has started while in the 1950s public works have been organized and coordinated at basin level for issues related to flood protection. Innovations in the post Second World War (1945-1970) aimed to develop an approach to sectorial

planning meeting the water demand of massive developing urban centers and providing solution to the dramatic changes occurring in economic, urban and social structure in Italy. Thus, specific water and soil management agencies have been created along with the institution of Hydraulic Works National Plans to guarantee water supply for urban, industrial and agricultural purposes as well as electric power generation and distribution (Massarutto et al., 2003). The creation of Regional Authorities in the 1970s coincides with the appearance of water quality as a major issue for water policy. Major achievements have been reached with the introduction of comprehensive legislation such as Water Resources and Soil Conservation Law (1989), Water Quality Management Framework Act (1999) and Wastewater and Nitrate Directives in (1999) that anticipated the most of the requirements of the Water Framework Directive issued in 2000 (Massarutto et al., 2003).

As well as other river basins in the North of Italy, Adige river basin earliest development has increased the use of large water amounts for hydropower generation and irrigation. Nowadays, in Alpine regions, intermittent hydropower generation has high economical relevance, being the most important renewable electricity source, with no CO^2 emission. Indeed, 28 large reservoirs are located in the mountainous area of the basin as well as in the central river stretch while downstream infrastructures are dedicated to irrigation and drinking water systems (Massarutto et al., 2003). Where is the prevalent use of water for hydropower generation and natural water flow is altered by the presence of dams and/or weirs, the stretch downstream of the dam is characterized not only by the reduction of the water flow, but also by the decrease of solid transport, as well as by massive bank protections that considerably alter daily variations to a considerable extent (DIAO, 2014).

2.2. Arno river basin and its regulatory framework

Arno River originates from the southern slope of Monte Falterona, in Tuscany (Italy), at the altitude of 1 385 m a.s.l.. The Arno river basin extends for around 8 228 km^2 with an altitude of the catchment area of 337 m a.s.l.. The flat areas (i.e. having 15 % of slope or less) represent 17 % of the entire basin.

The average annual temperature decreases gradually progressing from the sea to the inland areas of the basin while the annual temperature excursion amplitude varies due to altitude and proximity to the sea. Although in the Arno basin, there is a lack stations measuring wind speed and direction, it is still possible to get a sufficient representation of the movement of air masses that highlight the close relation between geographic and orographic location and the wind regime. In proximity of the coast, the prevailing winds blow from West and East according to seasonal

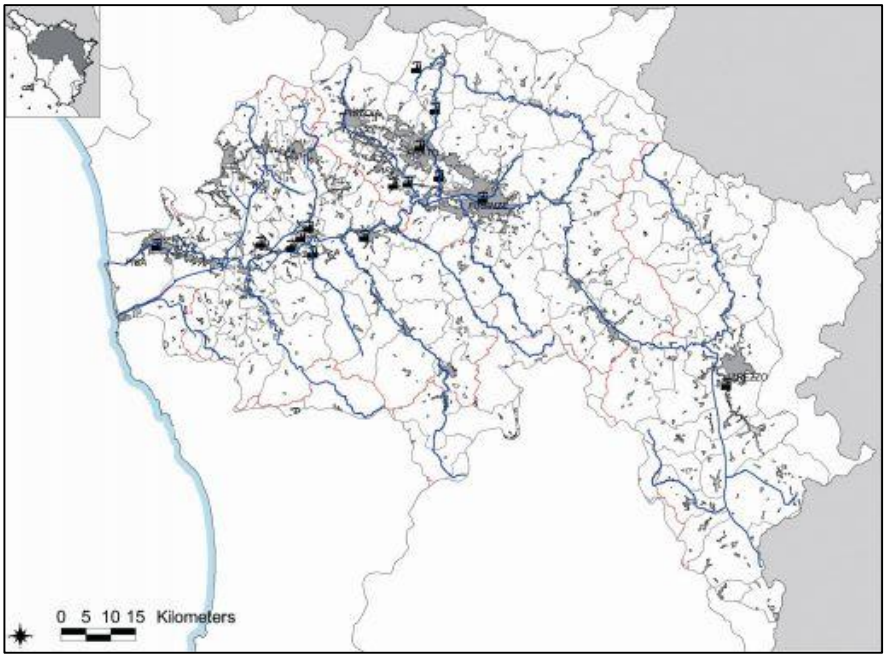

Figure 4: Arno river basin (Autorità di Bacino del Fiume Arno, 2014).

barometric changes that characterize the maritime areas of the Tyrrhenian coast (Regione Toscana, 2014).

In regard to the regulatory framework of Arno river basin, it is relevant to highlight that the first documented actions have been undertaken in the second half of the XIX century. In 1884 a specific law was oriented to the individuation of administrative procedures for the utilization or Arno waters. At the end of the 1950s the regulatory framework about the building and functioning of dams was defined and brought to the construction of dikes. However, the protection of Arno freshwaters in terms of quality and quantity has been promoted before the eventual occurrence of an intense exploitation. Indeed, in 1989, new rules were introduced to reset the organizational and functional framework for soil and water management. The main purposes of these rules were (and are still) oriented to the improvement of surface water and groundwater quality in order to avoid their degradation and the rationalization of surface water and groundwater uses in compliance with European and national directives (AdB Arno, 2014). In accordance with this legislation framework, from October 2007 Regione Toscana and other local authorities have started, in parallel, the projects of 12 mini-hydropower plants on Arno River, aiming to the generation of around 65 GWh per year (Provincia di Firenze, 2012).

2.3. Ebro river basin and its regulatory framework

The Ebro river basin covers 85 530 km^2 included between the southern-facing slopes of the Cantabrian Range and Pyrenees, with elevations over 3 400 m, and the northern-facing slopes of the Iberian Massif, with elevations up to 2 300 m . The Ebro river network includes more than 12,000 km of major streams. The outlet is located at Tortosa, about 180 km south of Barcelona (see Figure 5) (Batalla et al., 2003).

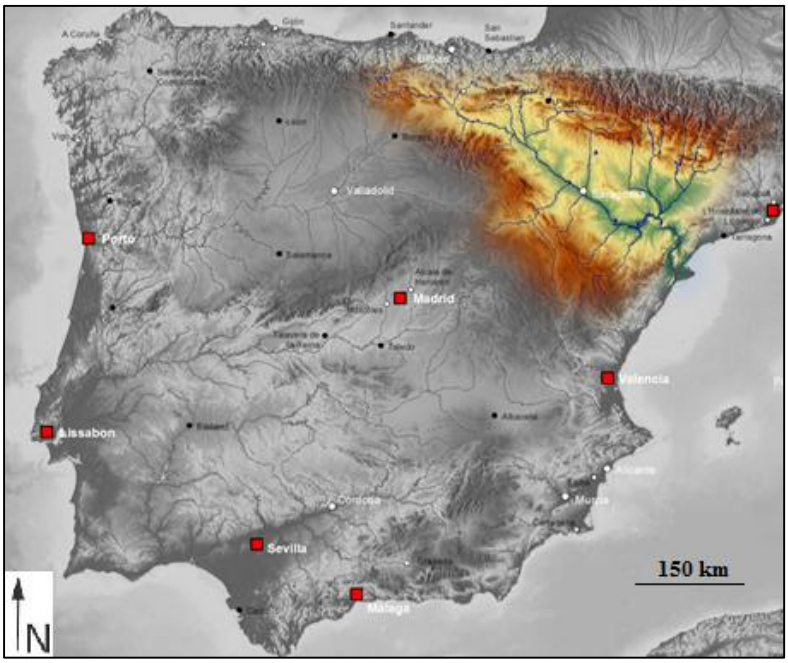

Figure 5: Ebro river basin (Wikimedia Commons, 2007)

From 1916 to 2000, 15 reservoirs larger than 100 hm^3 and 172 smaller reservoirs were constructed along the Ebro River and its tributaries. The total impoundment in the basin is estimated around 7 700 hm^3, equivalent to 57% of the river's average annual runoff (Batalla et al., 2003). Virtually, 67% of reservoir capacity built in the period 1950-1975, when 5 200 hm^3 of water was impounded and, even though none of the major dams was built for flood control, but the sheer volume of impoundments would likely affect flood magnitude. Water from reservoirs is mainly dedicated to hydropower generation, irrigation, cooling for nuclear plants and industrial and domestic uses (CHE, 1988). Indeed, on 1926 the Ebro Hydrographic Confederation has been created with the purpose of building regulatory framework for water uses for irrigation and electricity generation. In 2000, 240 running hydropower stations were producing 6,700 GWh per year (CHE, 2005). The regulation of the Ebro River, especially in the 1960s, had a direct influence on discharge pattern as reservoirs have produced substantial alterations to the flow regime on many rivers of the Ebro basin. However, according to by Garcıa et al. (2000) and the MIMAM (2000), although central and lower reaches of the Ebro

mainstream are slightly altered and the upper reach of the Ebro shows significantly altered fluvial regimes due to the impact of reservoirs, Ebro headwaters tributaries still maintain a natural flow regime.

2.4. Po river basin and its regulatory framework

The River Po extends for around 653 km and its covers an area of about 71,000 km^2 and includes 7 regions of Northern Italy: Lombardia, Piemonte, Liguria, Emilia Romagna, Veneto, Valle d'Aosta and Trentino Alto-Adige. It covers about 24 % of the Italian territory and it is densely populated, with a resident population of more than 16 million inhabitants (Artioli et al., 2005). The Po river valley hosts the principal productive areas of Italy as significant industrialization process has occurred in this area from the 1950s. Next to populated cities, heavy industry and intense agriculture are the principal users of fresh water. This situation has required in the last years the revision of actual resource use in order to monitor pollution load pressure and adopt new and more sustainable spatial planning strategies. The reception and implementation of the European Water Framework Directive (WFD) and the Directive on the assessment and management of flood risks would lead to a better management Po freshwaters in regards to their quality and quantity (AdB Po, 2009). Indeed, the impact of human settlement is nowadays high and entails the abstraction around 16.5 billion m^3 per year for agriculture and irrigation purposes, 2.5 billion m^3 for drinking water and 1.5 billion m^3 for industrial uses (W2A, 2014).

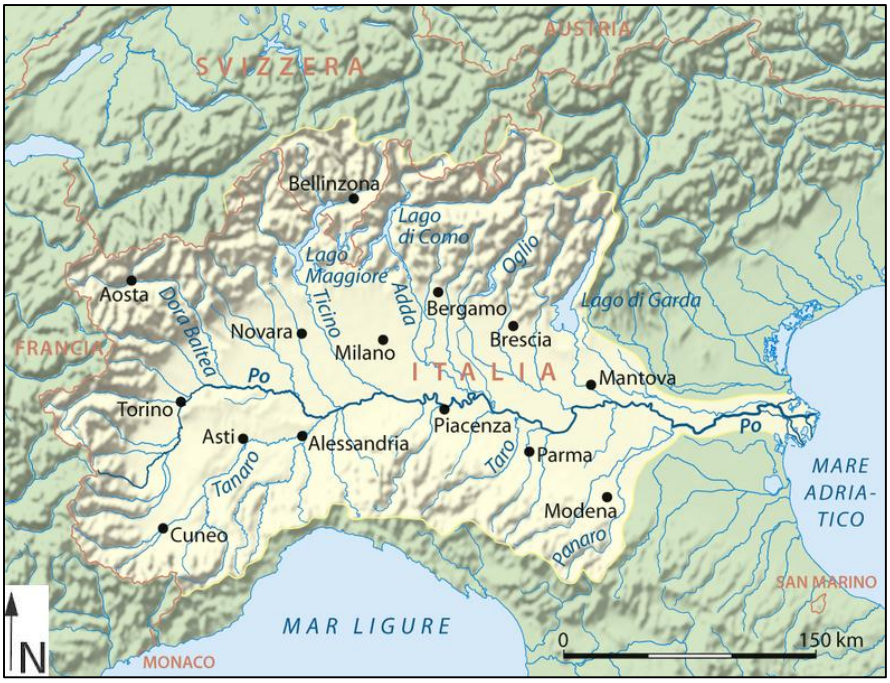

Figure 6: Po river basin (Wikipedia, 2014)

In the Alpine area, 2 803 billion m^3 a year are impounded in 174 artificial reservoirs, of which 143 are dedicated for hydropower production. Around 48 % of the national hydro-electric power production is generated within the Po valley (W2A, 2014). Although the river discharge variability is dominated by rainfall, the hydropower management has a direct influence on Po river discharge. Indeed, the river discharge is artificially kept low in summer by storing water in the reservoirs while a major water release occurs in winter for hydro-power generation. Camusso et al. (2001) have calculated that over a third of Po river discharge is affected by hydro-power reservoirs.

2.5. Rhone river basin and its regulatory framework

The Rhone is a major river system in the French Alps area; its basin covers around 98,000 km^2 of land in France and Switzerland. Rhone River is around 750 km long and receives 41 % of its total discharge comes from the Alps (EEA, 2009). Indeed, Rhone River originates from ice and snow melt from the Rhone Glacier and receives most of its water from Arve, Ain, Saône, Isère, Drôme, and Durance rivers. Figure 7 shows the origin of these major left tributaries which are strongly affected by water discharge from the French Alps (Souchon, 2004).

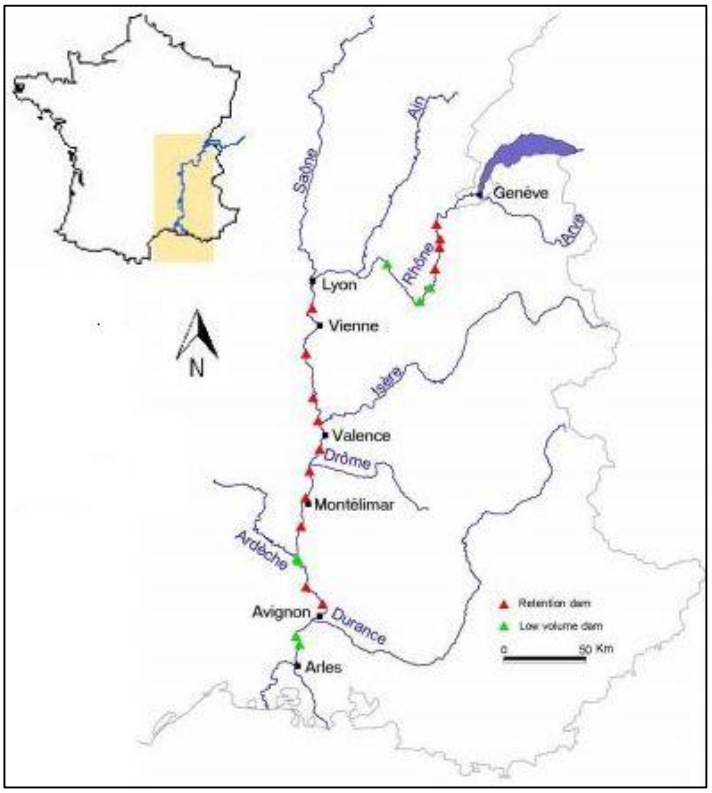

Figure 7: Rhone river basin (Souchon, 2004)

The river shows a relatively high gradient (i.e. 0,625 °/°°) and has been known for its poor navigability, but high hydroelectric potential. Indeed, while in the XVII century, human interventions started to modify the river by building levees flood defenses, from the XIX century the river has been object of interventions oriented to improve its navigability and several dams started to be built for irrigation purposes and hydropower generation. Nowadays, the flow regime of the Rhone is regulated by storage reservoirs that retain 7 billion m^3 of water, which constitute about 7.3 % of the annual runoff (Souchon, 2004).

The Rhone area, today densely populated (with around 3 million inhabitants) and significantly industrialized, has experienced an economic prosperity of the riverside cities and their inhabitants. In order to enhance water resources management of the Rhone basin, both national and European legal frameworks have been established with the intention to promote “healthy and running river” conditions. The freshwater fishing law (1984), The Water Law (1992) and the Water Framework Directive (2000) are examples of regulatory frameworks oriented to water resources restoration under a global watershed management perspective (Souchon, 2004).

3. Climate variability: Northern Hemisphere Teleconnection Patterns

Pressure dipoles are long distance climate phenomena (teleconnection) that are defined by anomalies of opposite polarity appearing at two distinct locations at the same time. Dipoles play a key role for the understanding of climate variability and are known to impact precipitation and temperature anomalies worldwide (Kawale et al., 2012). A teleconnection pattern is defined as a fixed spatial pattern associated to an index time series that evidence its evolution in terms of amplitude and phase (IPCC, 2007).

The different ways of patterns to occur affect climate and discharge variability over large areas. The example of Northern Atlantic Oscillation (NAO) is relevant: when it is in a positive phase (positive NAO-index, with a strong high pressure zone and a weak low pressure zone), the strong winds are west-directed towards Scandinavia, where the climate rounds to wet and mild, in opposition to Southern Europe where the climate becomes colder and dryer (Lindén et al., 2012). Specific studies have observed a significant increase in NAO index between the early 1970s and early 1990s corresponding to a long-term reduction in the Mediterranean winter discharge of about 1.7 X 10^3 m^3 s^{-1}, located mainly in the Gulf of Lion, Adriatic Sea and Balearic Sea (respectively outlets of Rhone, Po and Ebro rivers) (Struglia et al., 2004).

The influence regional rainfall regimes of such teleconnections have to be taken into account also by considering the concurrent state of two or more patterns. Zanchettin et a., 2007, discusses the dominant influence of the NAO and the impacts of El Niño–Southern Oscillation (ENSO) and Pacific Decadal Oscillation (PDO) on European rainfalls in wintertime. Although under strong NAO the response to ENSO anomalies is not significant, a weak NAO signal increases the influence of ENSO effects. It has been found that the coupling of ENSO and PDO identifies Central Europe as a sensitive area, where wet winters could be put in relation with strong ENSO events under positive phases of the PDO (Zanchettin et al., 2007).

These examples give an idea about the several aspects of teleconnection patterns that have to be further looked into in order to understand the behavior and characteristics of different patterns and their interactions. Thus, the continuous monitoring of teleconnection patterns is decisive to research about their role in the global climate system. For this study, the current known patterns that have an influence on the climate and weather in Mediterranean basin are presented.

3.1. East Atlantic

The East Atlantic (EA) pattern shows the effects of its low-frequency variability over the North Atlantic area and appears as a leading mode in all months. Its structure, similar to the NAO, and consists of a north-south gradient covering the North Atlantic from east to west. EA can be considered as a “southward shifted” NAO pattern because of the displacement of the anomaly centers southeastward to the approximate nodal lines of the NAO pattern (CPC, 2014). The positive phase of the EA index leads to above-average surface temperatures in Europe and it is also associated with above-average precipitation over northern Europe and Scandinavia, and with below-average precipitation across southern Europe.

Figure 9 shows the strong multi-decadal variability of EA index in the 1950-2014 time series, with the negative phase prevailing during in the 1950-1976 period, while the positive phase occurs between 1977 and 2004.

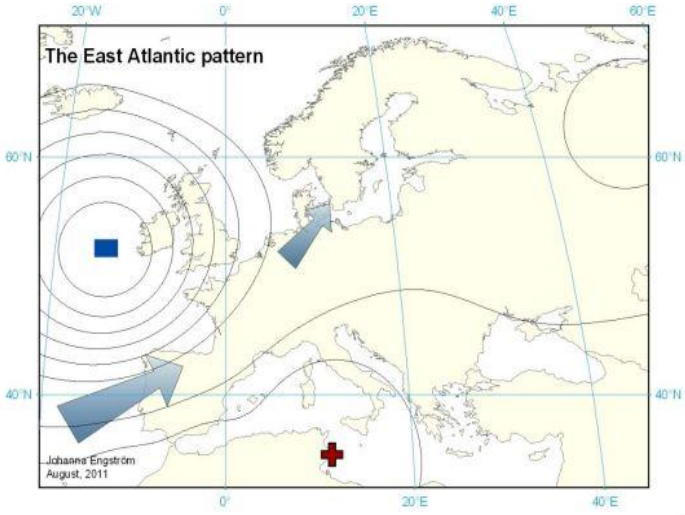

Figure 8: EA anomaly centers and atmospheric circulation directed, under the positive phase, towards northern Europe (Engström, 2011)

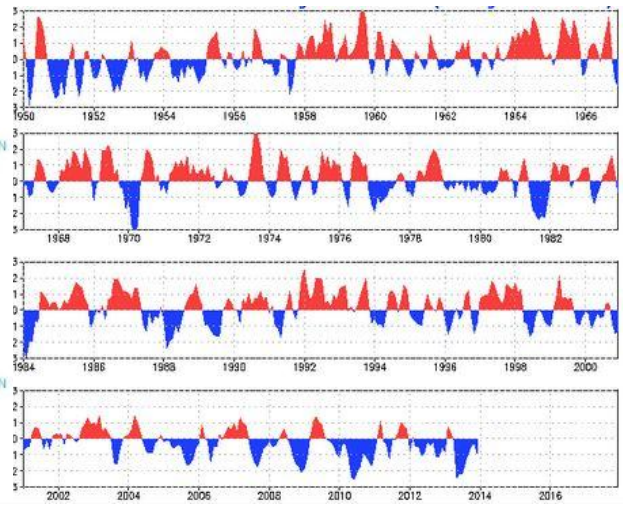

Figure 9: EA index time series (CPC, 2014a)

3.2. North Atlantic Oscillation

The North Atlantic Oscillation (NAO) teleconnection pattern is one of the most prominent teleconnection patterns, leading or significantly influencing the atmospheric circulation in nine out of twelve months and active all year around. (Barnston and Livezey, 1987).

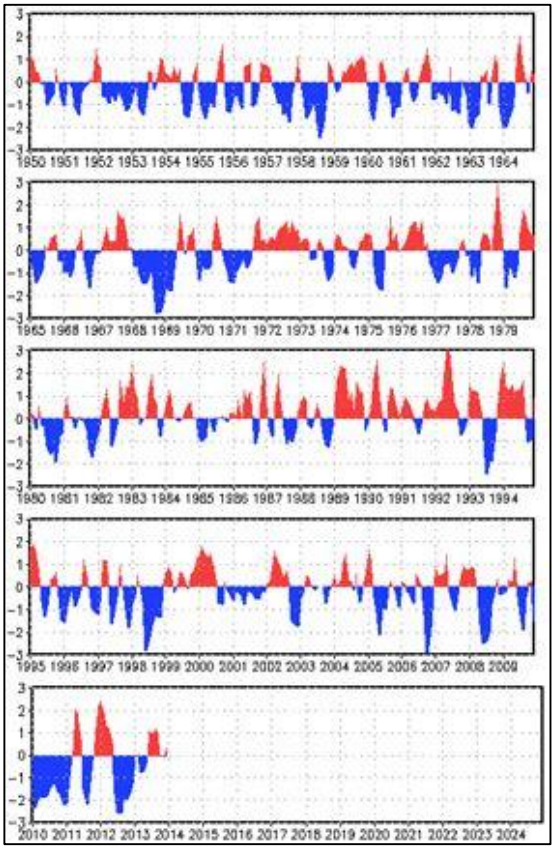

Figure 10: NAO index time series(CPC, 2014b)

The North Atlantic Oscillation index is expressed as the standardized difference of the surface sea-level pressure between the Azores High (subtropical region) and the Icelandic Low (subpolar region). Strong positive phases of NAO index lead to above-average temperatures over northern Europe and below-average temperatures in Greenland and oftentimes across southern Europe and the Middle East. Positive phases tend also to be associated with above-average precipitation over northern Europe and Scandinavia in winter, along with below-average precipitation over southern and central Europe. Opposite configurations related to temperature and precipitation anomalies have been observed during strong negative NAO index phases (CPC, 2014). Thus, both positive and negative phases of the NAO are associated with changes in the intensity and location of the North Atlantic jet stream and storm track that affect wide areas. Indeed, large-scale variations of the normal patterns of heat and moisture transport are responsible for temperature and precipitation patterns variability, extending from eastern North America to western and central Europe (CPC, 2014). Bouwer et al. (2008) individuated a major link between NAO index and precipitation variability during winter periods. Given the fact that river discharge in Europe during winter months (i.e. December, January and February) represents between the 23 and 43%

of total annual discharge in the major river basins, the analysis of NAO signal is of importance. Moreover, NAO index time series exhibits a significant interseasonal and interannual variability, and prolonged periods (several months) of both positive and negative phases of the pattern are common.

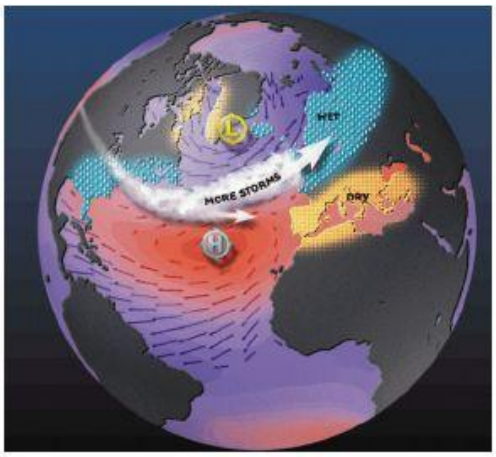

Figure 11: Positive NAO phase characterized by very low pressures in the subpolar region and very high pressures in the subtropical region (Bell, 2009)

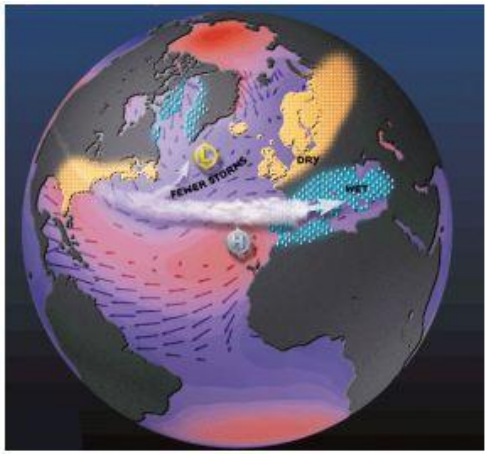

Figure 12: Negative NAO phase characterized by weak low pressures in the subpolar region and weak high pressures in the subtropical region (Bell, 2009)

3.3. Scandinavia

The Scandinavia pattern (SCAND) consists of a primary circulation center extended over Scandinavia and large portions of the Arctic Ocean north of Siberia: weaker centers having of opposite signs are located over Western Europe and western Mongolia (CPC, 2014b).

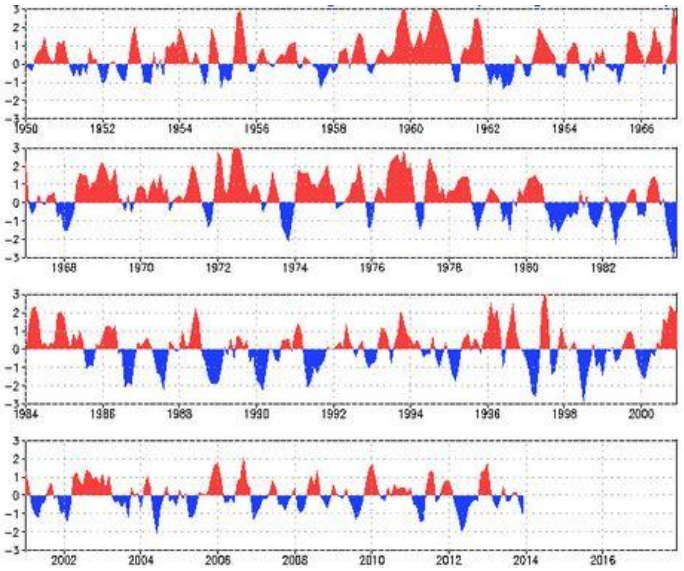

Figure 13: Scandinavia index time series (CPC, 2014c)

Ciccarelli et al. (2008), have found that positive phases of the Scandinavian pattern, along with and the presence of blocking episodes (i.e. interruption of the normal zonal flow is interrupted by meridional flow) are correlated with an increase in precipitation and decrease in temperature especially during summer and fall periods and cold temperatures in Mediterranean basin, more specifically in north-western Italy. This observation is confirmed also by Bueh et al. (2007) who individuate a correlation between the positive phases Scandinavia pattern and the observation of below-normal temperatures across Western Europe, above-normal precipitation across southern Europe, and dry conditions over the Scandinavian region.

3.4. Pacific Decadal Oscillation

The Pacific Decadal Oscillation is identified with low frequency variations in the leading of sea surface temperature (Zanchettin et al., 2007) and its variability shows similarities with El Niño–Southern Oscillation (ENSO) (see Figure 14), although it varies over a longer period. Indeed, the PDO can linger on the same positive or negative phase for 20-30 years, while ENSO periodicity usually lasts for 6 to 18 months. The variation of PDO can be monitored through PDO index, defined as the projections of winter mean sea surface temperature (SST) anomalies onto their first empirical orthogonal function vectors in the North Pacific area (north of 20º parallel).

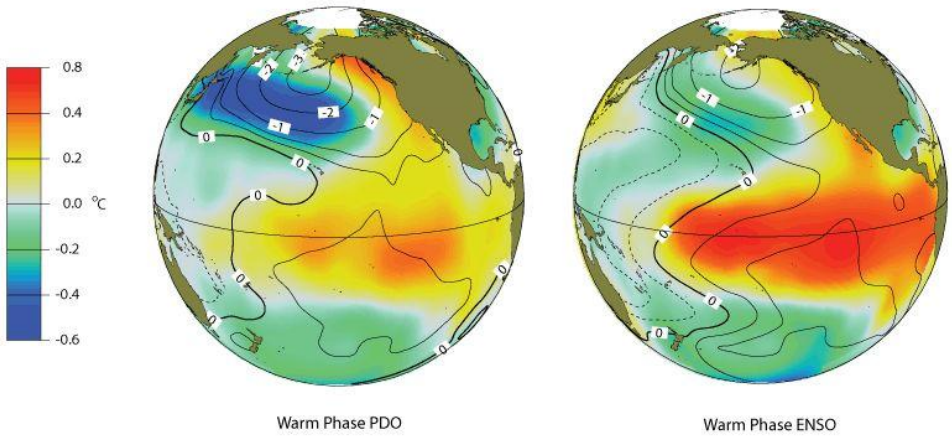

Figure 14: regional similarities in warm PDO and ENSO phases (Climate Impact Group, University of Washington, 2014)

The PDO, similarly to ENSO, consists of a warm and cool phase which has an effect on upper level atmospheric winds. Whenever the PDO phase changes, significant implications are registered in relation to global climate, Pacific and Atlantic hurricane activity, droughts and flooding, the productivity of Pacific basin marine ecosystems, and global land temperature patterns (North Carolina Climate Office, 2014). The way ENSO and PDO relate to each other is still uncertain. However, Zanchettin et al. (2007) show how the intensity of ENSO has an impact on European rainfalls during winter periods: indeed, given weak intensity phases of NAO pattern, there is a switching behavior of ENSO effects driven by periodical SST anomalies that characterize PDO.

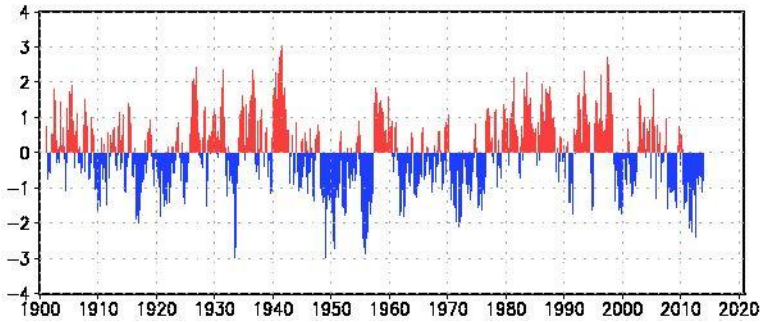

Figure 15: PDO index time series (Tokyo Climate Center, 2014)

4. Data

4.1. River discharge time series

The first issue in evaluating which rivers could be taken into account for this study was concerning the detection anthropogenic effects on river flow. Rivers with no regulation, or at least negligible regulation, are the only ones that can be considered to estimate the variability of natural continental discharge in the Mediterranean basin. As described in section 2., Rhone, Po and the Nile rivers Major overall contribute to continental discharge to the Mediterranean basin while secondary inputs are from Ebro, Adige (Struglia et al., 2004) and Arno rivers.

However, although the contribution of river Nile discharge, estimated around 1200 m^3s^{-1} at its outlet (Struglia et al., 2004), is relevant for the hydrological balance of the Mediterranean Sea, Nile river is not object of this study because of the heavy regulation that has distorted the natural seasonal discharge of its waters over decades. Processes that naturally affect freshwater discharge such as changes in precipitation regimes, in evaporation and catchment vegetation have been altered by the anthropogenic control on total Nile discharge. The purposes of such intervention are well known and range from hydropower generation to water extraction for domestic, agricultural and industrial uses (Howell et al., 1994).

Regulatory framework is also improving in the Balkans area (i.e. Albania, Kosovo, Montenegro, Serbia, Bosnia and Herzegovina and Macedonia): the Balkans Renewable Energy Program (BREP) is going to have a relevant impact especially on the region of Western Balkans which has natural potential for the development of small hydro power plans as a source of electricity. Although rivers from the Balkans area could be considered object of study (as the regulation processes have started to affect the natural river discharge only during the last years), the unavailability of discharge data over long periods (i.e. at least 50 years) makes impossible the analysis and comparison with discharge time series of other rivers in the Mediterranean basin.

The selected Rivers are listed in Table, along with the relative name of the outlet rivers´ station where flow measurements have been performed.

River	Outlet station	Time series	Data Source
Adige	*Boara Pisani*	*1922-2008*	*ARPA Veneto*
Arno	*San Giovanni alla Vena*	*1960-2012*	*Autorità di Bacino Arno*
Ebro	*Tortosa*	*1952-2012*	*Confederación Hidrográfica del Ebro*
Po	*Pontelagoscuro*	*1919-2012*	*ARPA Emilia Romagna*
Rhone	*Beaucaire*	*1921-2012*	*Compagnie Nationale du Rhône*

Table 1: Selected Rivers

4.2. Teleconnection patterns time series

The identification of the Northern Hemisphere teleconnection indices for this study uses the Rotated Principal Component Analysis (RPCA) technique (Barnston et al., 1987). RPCA is useful to isolate the primary teleconnection patterns for each month of the year and construct time series of each pattern. The Climate Prediction Center (source of NAO, EA and SCAND time series) applies the RPCA method to monthly mean standardized 500-mb height anomalies obtained from the Climate Data Assimilation System in the area included between 20°N-90°N from January 1950 to December 2012. Height anomalies are standardized by the monthly means and standard deviations observed in the period 1950-2012 (CPC, 2014c).

To what concern PDO, it is usually monitored by using an index that is calculated by spatially averaging the monthly SST of the Pacific Ocean north of 20°N. The monthly mean global average SST anomalies are then removed to avoid any disturbance due to "global warming" signals that may be present in the data. PDO teleconnection pattern time series ranges from 1900 to 2012. As teleconnection patterns reflect large-scale changes in the atmospheric circulation over long time periods, the availability of long time series is decisive for the analysis proposed by this study.

Teleconnection pattern	*Time series*	*Source*
EA	*1950-2012*	*Climate Prediction Center - NOAA*
NAO	*1950-2012*	*Climate Prediction Center - NOAA*
SCAND	*1950-2012*	*Climate Prediction Center - NOAA*
PDO	*1900-2012*	*JISAO - Washington*

Table 2: Selected teleconnection patterns

5. Methodology

The hydrological cycle is the perpetual movement that involves the circulation of water in the Earth-atmosphere system. Large scale atmospheric and oceanic circulations have a strong impact on the variability of the main component of the hydrological cycle. Because of the complexity of the hydrological processes over continental areas, in this report discharge time series are used to deduce its variability from. Indeed, the analysis of river discharge includes many other hydrological factors such as precipitation, temperature, interception and solar radiation fluctuations that directly influence losses by evapotranspiration. Thus, time series of freshwater discharge at the outlet of river basins are hereby used to evaluate gain and losses in the continental water cycle.

Long-term river discharge and teleconnection pattern time series are studied using wavelet transform method. Wavelet transforms can be divided in 2 classes: the Continuous Wavelet Transform (CWT) and Discrete Wavelet Transform (DWT). As DWT is mainly used for noise reduction and data compression, while CWT is a common tool to extract signals from time series and to analyze localized intermittent oscillations, this study will be focusing on this last class, which is more indicated for feature extraction purposes (Grinsted et al., 2004). Then cross wavelet technique is applied to examine coherence and phase relations between pairs of time-series on interannual scale to find individuate the teleconnection pattern signal in river discharge data. Cross-wavelet analysis identifies regions where time series have common power, whereas wavelet coherence identifies regions where time series show correlated (or coherent) fluctuations (Cazelles et al., 2008; Grinsted et al., 2004). All the analyses were carried out using a MatLab software package written by Torrence and Compo (available at "http://atoc.colorado.edu/research/wavelets/''). Specific codes for the performance of wavelet and cross wavelet analyses are reported in Appendix 1.

5.1. Wavelet analysis

The wavelet transform technique was introduced and formulated by Morlet et al. (1982) and Grossmann and Morlet (1984). In the wavelet analysis, both time and frequency variations of a non-stationary time series are investigated. A wavelet analysis decomposes a time series into scale components allowing distinction between the oscillations that occur at fast scales and the ones that occur at slow scales. The main property is that wavelet functions, unlike other spectral techniques (such as the Fourier and Gabor transforms), allow to keep information about the occurrence of non-stationary events in both time and frequency domains, highlighting localized intermittent periodicities. Wavelet analysis provides also additional information about the level of significance by varying the period in accordance to fast and low scale oscillations (Grinstead et al., 2004).

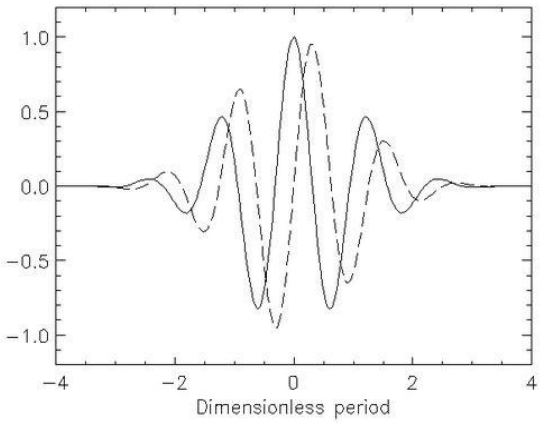

Figure 16: Morlet wavelet (Torrence and Compo, 1998)

A wavelet function is characterized by zero mean and its localization in both frequency and time. One particular wavelet function, the Morlet (Ψ_0), was used in this study since it is the most indicated wavelet for extracting features, maintaining a good balance between frequency and time information (Grinstead et al., 2004). It is defined as

$$\Psi_0(\eta) = \pi^{-1/4} e^{i\omega_0 \eta} e^{-\eta^2/2} \quad : \qquad \textit{(Eq. 1)}$$

where η and ω_0 are, respectively, non-dimensional time and non-dimensional frequency. Since Morlet wavelets contain several oscillations (see Figure 16), both positive and negative peaks are combined in the wavelet power and considered in the analyses (Torrence and Compo, 1998).

Continuous wavelet analyses were performed for the available time period of each river discharge and teleconnection pattern time series. The cone of influence, indicated with a lighter shade outside, highlights the area of the graph where the power spectrum might be distorted since the wavelet is not completely localized in time (Lidén et al., 2012).
Wavelet power spectra, ranging from 1/8 to 4 values (respectively indicated in blue and orange), have been examined for all the selected rivers, whose discharge data are standardized by daily means and standard deviations observed in the relative monitoring period. A similar process has been used for the analysis of teleconnection patterns: here the standardization was done by monthly means registered during the monitoring periods.

For a correct interpretation of wavelet-based statistical results of non-stationary events, significance tests cannot be omitted. The statistical significance level of the wavelet power is estimated by using Monte Carlo method. The generation of a large ensemble of data set pairs constitutes the basis for the calculation of the wavelet coherence. The Monte Carlo estimation of significance level requires around 1000 surrogate data set pairs (Grinsted et al., 2004). By performing Monte Carlo method it is possible to compute the 95% confidence interval, highlighted with black solid contours (see Figure 17).

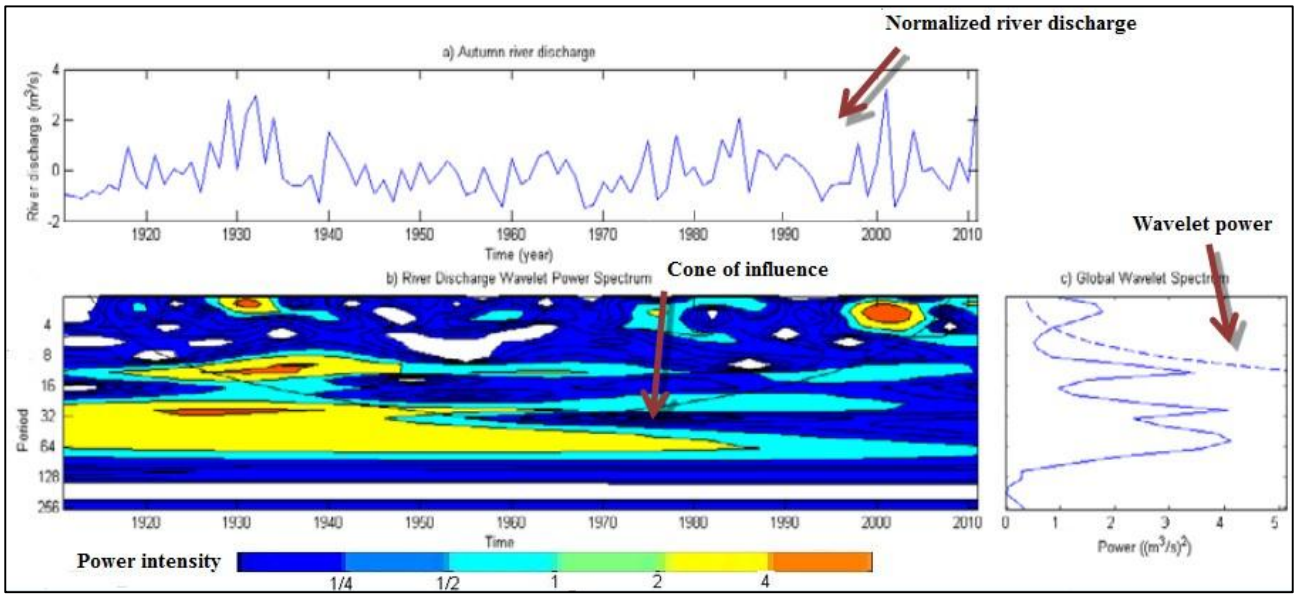

Figure 17: River discharge wavelet analysis (Lidén et at., 2012)

5.2. Cross wavelet analysis

From two CWTs we construct the Cross Wavelet Transform (XWT) which is a powerful method for showing eventual relations between two time series, as it exposes their common power and relative phase in time-frequency space. The cross wavelet transform (XWT), on the basis of two time series (x and y), is defined as $W^{XY}=W^{X}W^{Y}$ *, where * denotes complex conjugation and the cross-wavelet power, $|W^{XY}|$, indicates areas having high common power between time series x and y (Grinsted et al., 2004). Obviously, cross wavelet analysis can be performed only if two time series are extended over the same time period.

As it is interesting to understand the phase difference between the components of the two time series, there is the necessity to estimate the mean of the phase difference. Zar (1999) defines the circular mean of a set of angles (a_i, i=1...n) as

$$a_m = \arg(X, Y) \text{ with } X = \sum_{i=1}^{n} \cos(a_i) \text{ and } Y = \sum_{i=1}^{n} \sin(a_i), \quad : \qquad \textit{Eq. 2}$$

Although it is difficult to calculate the confidence interval of the mean angle reliably (especially because the phase angles are not independent), the arrows in the graph show where the two wavelet transforms are in phase or anti-phase, pointing respectively to the right or to the left (see Figure 18).

The cone of influence, as described in section 5.1., highlights the area of the graph having major statistical significance because of the data availability over a certain time period. The black contours highlight statistically significant wavelet power at the 5% level of a red noise process.

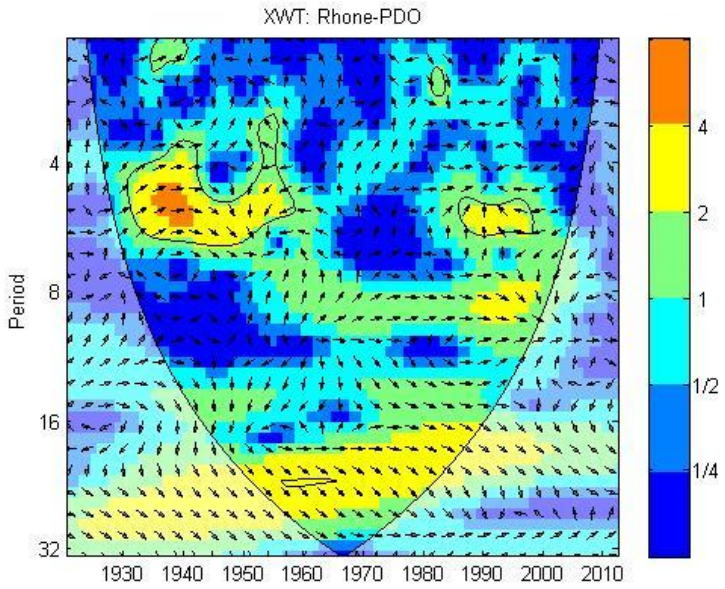

Figure 18: Rhone river discharge and PDO index cross-wavelet analysis. It is possible to note the COI, the black solid contours highlighting 5% significance level and the power intensity scale

6. Results

In this section, the relations between the outlined river discharge time series and large-scale atmospheric circulation patterns are investigated by means of wavelet and cross wavelet analyses. The results of this study are presented focusing on single river discharge time series as well as teleconnection patterns time series. Matlab figures show wavelet and cross wavelet analyses of the above-mentioned time series. Wavelet analysis of each river discharge time series is cross-checked with wavelet analyses of the four selected teleconnection pattern time series, searching for climate variability influence on river discharge in the Mediterranean basin.

6.1. Wavelet analysis results

6.1.1. River discharge time series

The Continuous Wavelet Transform (CWT) of Adige time series shows high power in the ≈2, ≈10 and ≈20 year periods. High spectrum power in the last two mentioned year periods is found both within and outside the cone of influence.

Wavelet coherence 5% significance level is obtained in correspondence of the ≈ 2 year period around early 1950s, late 1970s and 2000.

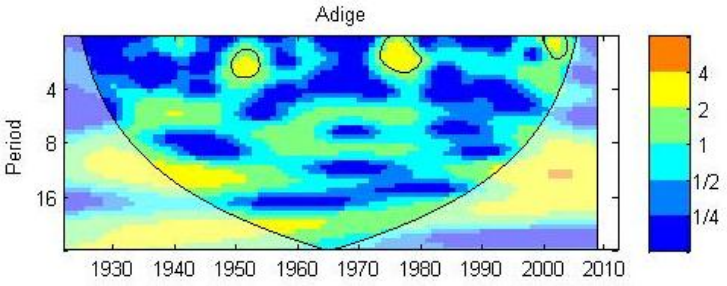

Figure 19: Adige river discharge wavelet analysis

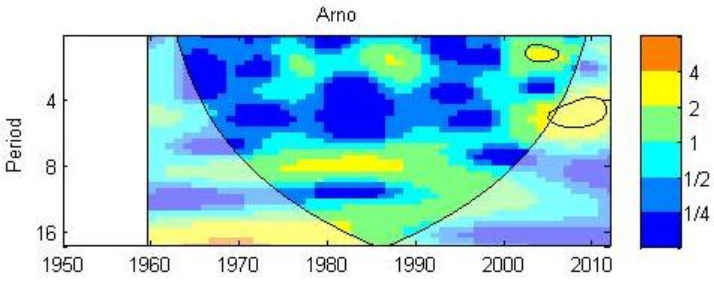

Figure 20: Arno river discharge wavelet analysis

The CTW of Arno discharge time series shows high power in the ≈ 2, ≈ 5 and 8 year periods. The relative short discharge time series, covering the period 1960-2012, does not allow getting relevant information about period year periods over 16 years. Although it is possible to foresee high power signal also in the ≈ 20 year period, only further extension of current discharge time series could confirm this information. Wavelet coherence 5% significance level is obtained in correspondence of the ≈ 2 year period around 2005 and in correspondence of the ≈ 5 year period, partly outside the cone of influence, around 2005-2010.

Figure 21 shows high power in the ≈ 8, year period, although in this information is not highlighted by the 5% significance level. The outlined significance level is obtained in correspondence of the ≈ 2 year period around 1990, where the spectrum power value is 1.

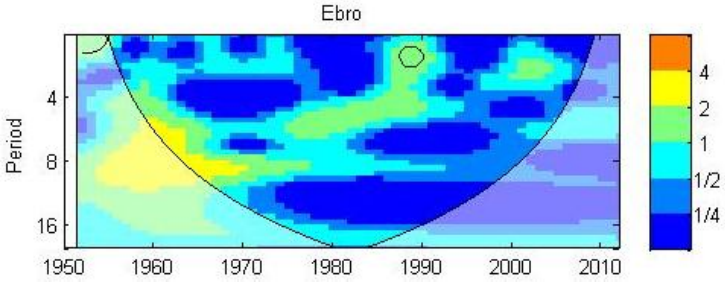

Figure 21: Ebro river discharge wavelet analysis

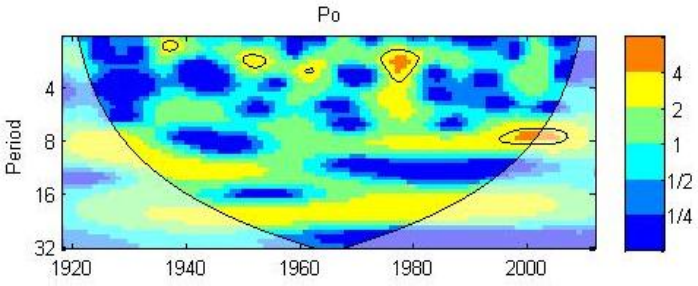

Figure 22: Po river discharge wavelet analysis

The CTW of Po discharge time series shows high power in the ≈ 2, 4-8 and ≈20 year periods. The latter year period shows very clearly the high value of the power spectrum over a period between 1935 and 2005. Wavelet coherence 5% significance level is obtained in correspondence of the ≈ 2 year period around 1938, 1952, 1960 and late 1970s. The 5% significance level is also found in correspondence of the 8 year period over 2000s.

The CTW of Rhone discharge time series shows high power in the ≈2, 4-8 and 16-25 year periods. Similarly to Po river discharge wavelet analysis the latter year period presents high power values over a long period between 1930 and 2008. The 5% significance level is obtained in the 4-8 year period in correspondence of 1930-1948 period and late 1990s as well as in the ≈16 year period in correspondence of the period 1978-1998.

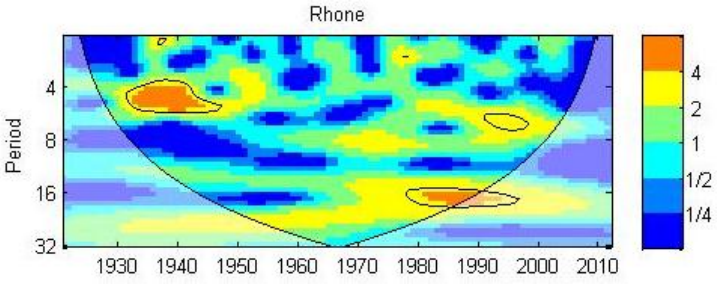

Figure 23: Rhone river discharge wavelet analysis

6.1.2. Teleconnection patterns time series

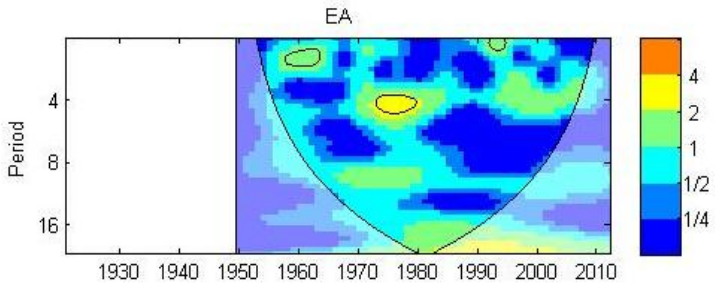

Figure 24: East Atlantic teleconnection pattern wavelet analysis

The CWT of East Atlantic teleconnection pattern shows high power in the 4 year period, while lower but still relevant power is found in the ≈8 year period. It could be possible to foresee high power also in the ≈ 20 year period, but the information is not validated within the cone of influence of EA wavelet analysis. Wavelet coherence 5 % significance level is obtained in correspondence of the ≈1, ≈2 and 4 year periods, respectively around 1993, early 1960s and late 1970s.

In Figure 25 it is shown that CWT of North Atlantic Oscillation teleconnection pattern exhibits high power in the ≈2 and 10-16 year periods, while lower power values are found in the 4-6 year period. Wavelet coherence 5 % significance level is observed in correspondence of the ≈2 year period around 1970. Moreover, it is found in correspondence of the ≈2 year period around 2010 as well as in correspondence of ≈15 year period around 2000. However, these latter findings are located outside the cone of influence (see Figure 25).

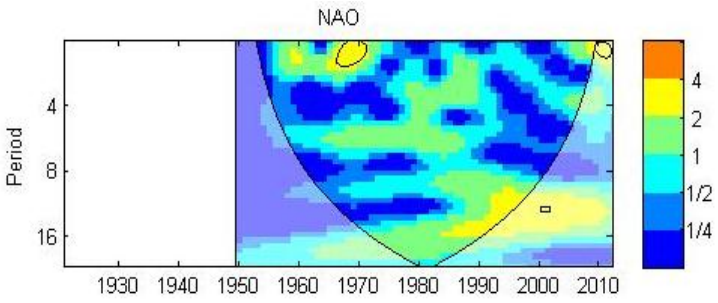

Figure 25: NAO teleconnection pattern wavelet analysis

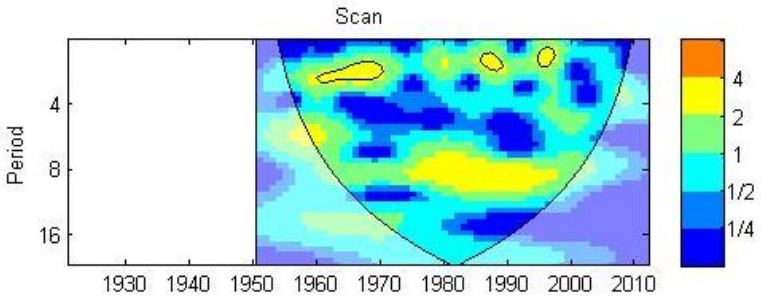

Figure 26 displays the CWT of Scandinavia teleconnection pattern. High power values are found in the ≈ 2, ≈ 6 and ≈ 8 year periods. However, the 5% significance level is obtained only in correspondence of the ≈ 2 year period from 1960 to 1970, around late 1980s and around mid-1990s.

Figure 26: Scandinavia teleconnection pattern wavelet analysis

The CWT of PDO index shows high power in the ≈6, 8-10 and 20-30 year periods. This result seems to confirm the theory about PDO low frequency phase variations that occur over longer periods (typically around 20-30 years). Wavelet coherence 5% significance level is obtained in correspondence of the ≈2 year period, around 1930, and in correspondence of the 4-6 year period, from 1930 to 1960 and from 1990 to 2000.

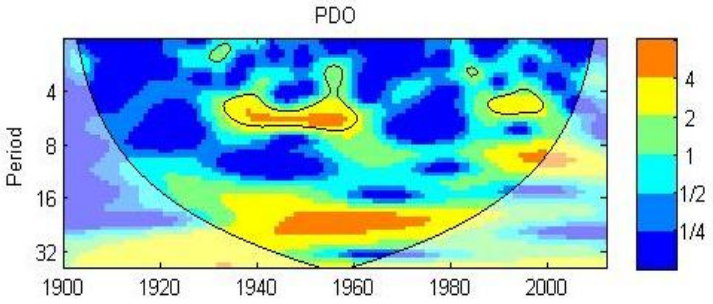

Figure 27: PDO index wavelet analysis

6.2. Cross Wavelet Analysis

6.2.1. Adige

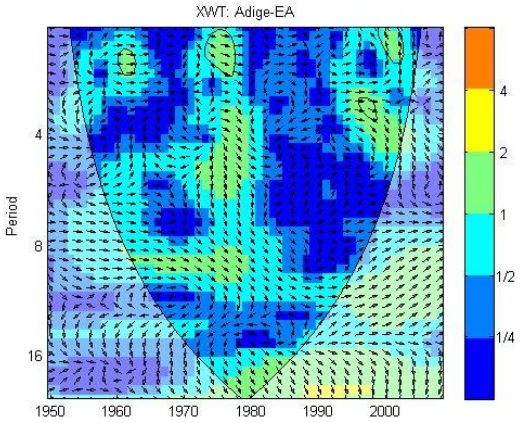

Figure 28: Adige and NAO cross wavelet analysis

Figure 28 shows XWT results by using the standardized Adige river discharge and EA teleconnection pattern time series. Power 1 values are obtained in the ≈2, 4-6 and ≈8 year periods while higher power values can be foreseen outside the cone of influence. The 5% significance level is found in correspondence of the ≈2 year period, around 1963, 1975 and 2000 and in correspondence of the ≈4 year period around 1997. In three of the four listed cases, the events are in phase, as shown by the right-pointing arrows.

The XWT of the standardized Adige river discharge and North Atlantic Oscillation teleconnection pattern time series shows power 1 in ≈2, ≈6 and 12-16 year periods. Higher power values are registered outside the cone of influence, in the 12-16 year period. This information is validated by the 5% significance level while significance of wavelet power is also found in the ≈2 year period around 1978. The XWT show different signals concerning the phase or anti-phase behavior of Adige river discharge and NAO. Indeed, in the ≈6 year period, arrows clearly point to the right while in the ≈2 year period arrows don't exhibit a leading direction.

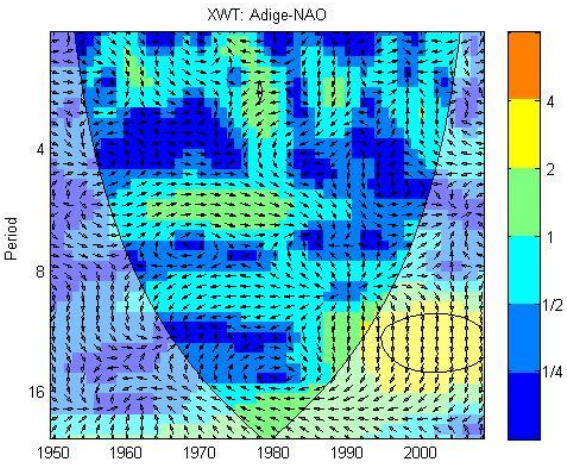

Figure 29: Adige and NAO cross wavelet analysis

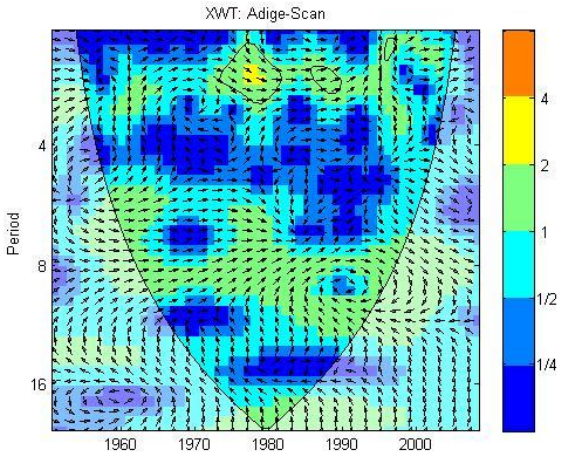

Figure 30: Adige and Scandinavia cross wavelet analysis

The ≈2 year period of Adige river discharge and Scandinavia XWT exhibits high power values. This information is also accompanied by the individuation of the 5% significance level that is shown in the period 1970-1980 and around late 1980s. In these periods, the study highlights that Adige river discharge and NAO index are in phase. Power 1 values are individuated in the ≈8 year period and can be foreseen in the ≈20 year period.

Figure 31 shows XWT results by using the standardized Adige river discharge and PDO index time series. High power values are obtained in the ≈6, ≈10 and ≈20 year periods. The 5% significance level is found in correspondence of the ≈2 year period, around 1955 and 1975 and in correspondence of the ≈6 year period in the period between 1935 and 1945. In these areas of the graph, the right-pointing arrows indicate that Adige river discharge and PDO index are in phase. Wavelet coherence 5% significance level is also obtained in correspondence of the ≈10 year period, around early 2000s, outside the cone of influence.

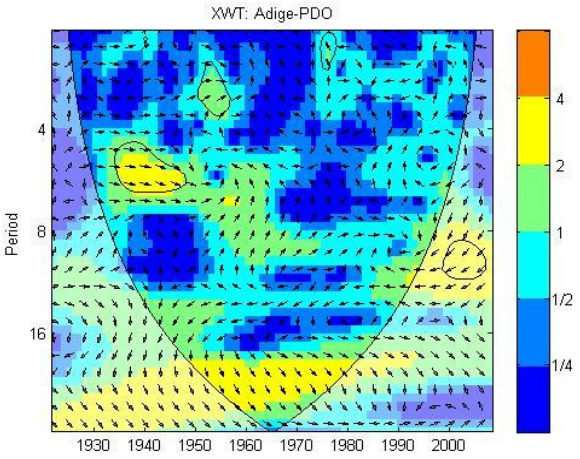

Figure 31: Adige and PDO index cross wavelet analysis

6.2.2. Arno

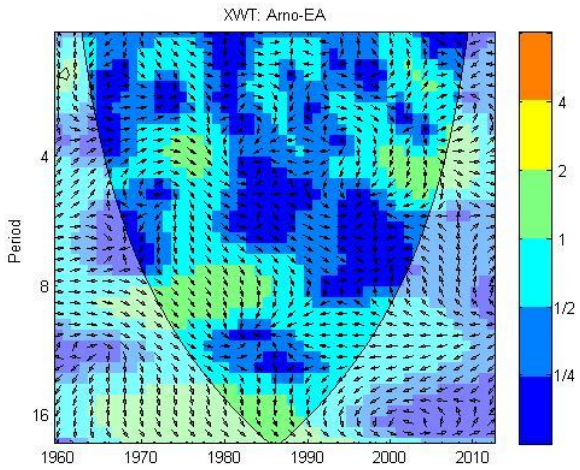

Figure 32: Arno and EA cross wavelet analysis

The Cross Wavelet Transform (XWT) of the standardized Arno discharge and East Atlantic teleconnection pattern time series does not show any region having relatively high power values. Three year periods (i.e. ≈4, ≈8 and ≈16) show power 1 respectively in correspondence of 1975 and 2005, 1970-1980 and 1965-1990 periods. This information is partially located outside the cone of influence of XWT analysis (see Figure 32). The 5% significance level is not found in this specific case and the arrows (with in-phase pointing right, anti-phase pointing left) don't show a leading direction, not allowing any significant observation about the correlation of the two analyzed events.

The Cross Wavelet Transform (XWT) of the standardized Arno discharge and North Atlantic Oscillation teleconnection pattern time series shows power 1 in ≈2, 6-16 year periods. It is possible to foresee high power signal also in the ≈16 year period but only further extension of analyzed time series could confirm this information. Wavelet coherence 5% significance level is obtained in correspondence the ≈2 year period, around 1990 where the arrows do point downward left, indicating possible interference in the anti-phase correlation of the two analyzed non-stationary events.

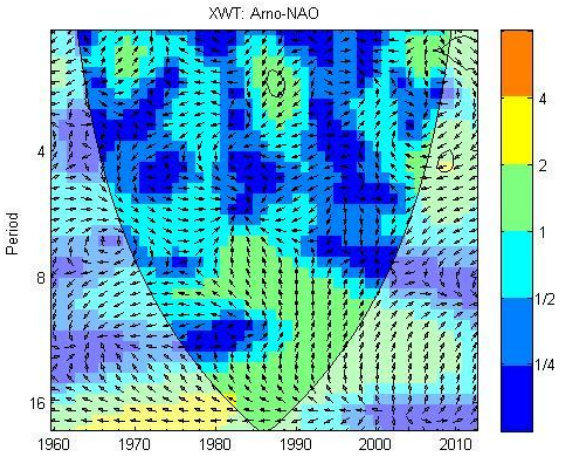

Figure 33: Arno and NAO cross wavelet analysis

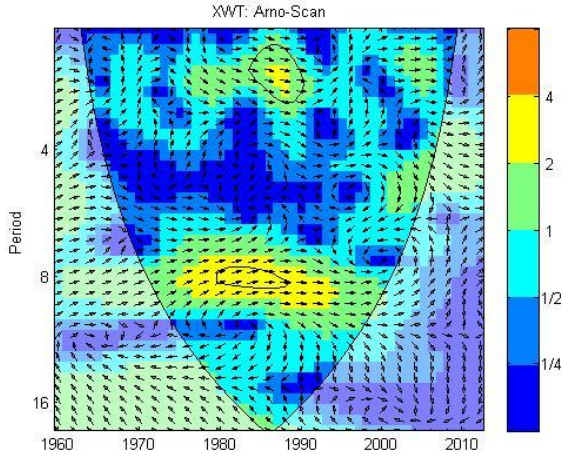

Figure 34: Arno and Scandinavia cross wavelet analysis

The Cross Wavelet Transform (XWT) of the standardized Arno river discharge and Scandinavia teleconnection pattern time series shows high power in ≈2 and ≈8 year periods. This information is also validated by the 5% significance level respectively around 1990 and the period 1980-1990 (see Figure 34). In both year periods, the pointing-right arrows show that the two events are in phase, i.e. under positive phases of Scandinavia pattern there is also an increase in Arno river discharge.

Figure 35 shows XWT results by using the standardized Arno river discharge and Pacific Decadal Oscillation index time series. Higher power values are obtained in the 8-10 year period and can be foreseen in the >16 year period. The 5% significance level is found in correspondence of the ≈2 year period, around 1985 where the arrows point to the left, showing the Arno river discharge and PDO anti-phase conditions.

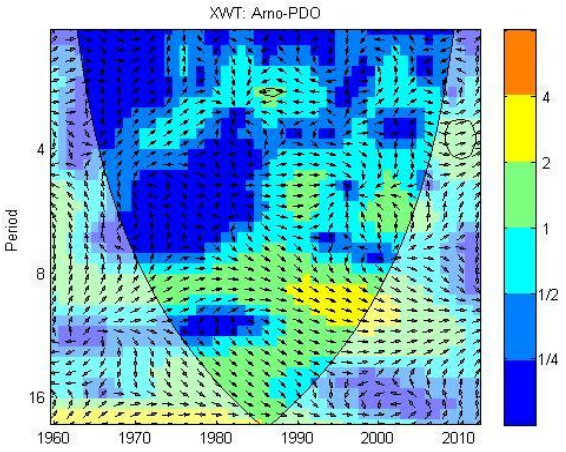

Figure 35: Arno and PDO cross wavelet analysis

6.2.3. Ebro

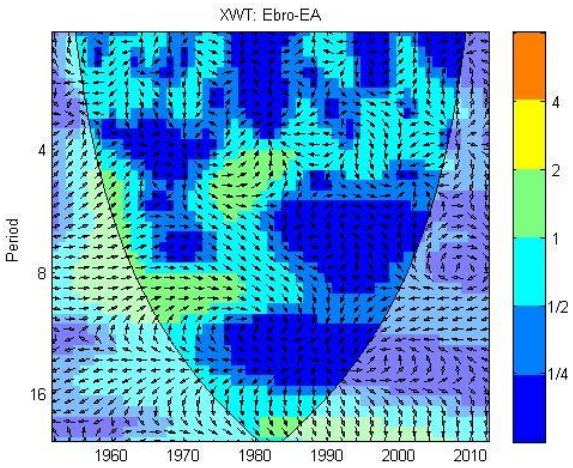

Figure 36: EBRO and EA cross wavelet analysis

The XWT of the standardized Ebro river discharge and East Atlantic teleconnection pattern time series shows power 1 in the 4-8 year period. However, this information is related to the period between 1960 and 1980, while in recent years the wavelet power is considerably lower. It is possible to foresee power 1 value also in the ≈16 year period, but as this signal is partially registered within the cone of influence. Thus, speculations cannot be done in regard to the phase or anti-phase behavior of the analyzed non-stationary events also because the arrows in the graph do not show a leading direction.

Figure 37 shows XWT results by using the standardized Ebro river discharge and NAO teleconnection pattern time series. Power 1 values are obtained in the 2-6, ≈10 and ≈20 year periods. The 5% significance level is found in correspondence of the ≈2 year period, around 1968 and 1988. However, no speculations can be done in regard to the phase or anti-phase behavior of the analyzed time series also because the arrows in the graph do not show a leading direction.

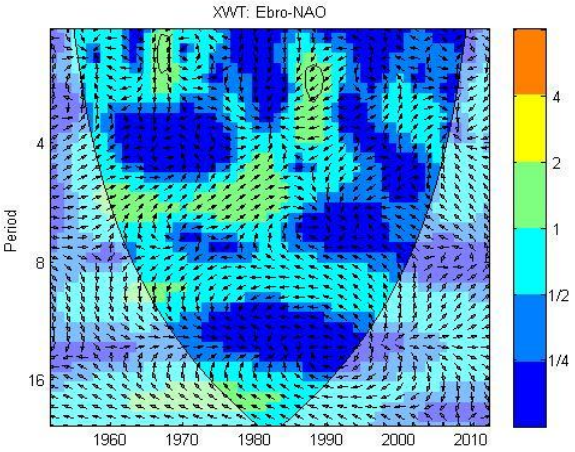

Figure 37: Ebro and NAO cross wavelet analysis

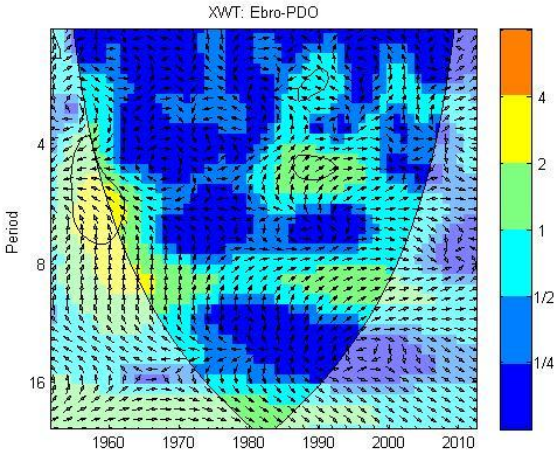

Figure 38: Ebro and PDO index cross wavelet analysis

The XWT of the standardized Ebro river discharge and PDO index time series shows high power in the ≈2 and 4-8 year periods. In correspondence of the latter, the 5% significance level is found between 1955 and 1965, partly outside the cone of influence, while around the late 1980s, the significance level is highlighted both in the ≈2 and ≈5 year periods. The results concerning phase or anti-phase behavior of the analyzed time series are conflicting since the arrows point in different direction in the same year period (e.g. ≈5 year period).

The ≈2 year period of Ebro river discharge and Scandinavia XWT exhibits power 1 values. This information is also accompanied by the individuation of the 5% significance level that is shown in the early and late 1960s as well as in the late 1980s. The ≈6 and ≈8 year periods show even higher power values and the 5% significance level is obtained around 1960. In these periods, the study highlights that Adige river discharge and Scandinavia index are in phase.

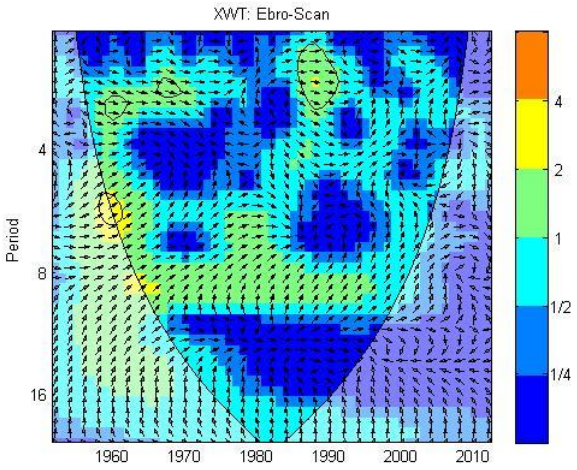

Figure 39: Ebro and Scandinavia pattern cross wavelet analysis

6.2.4. Po

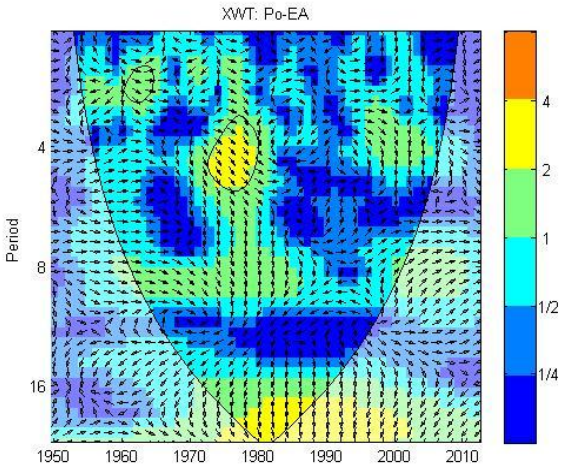

Figure 40: Po and EA pattern cross wavelet analysis

The XWT of the standardized Po river discharge and EA teleconnection pattern time series shows high power in the ≈4 and ≈20 year periods. In correspondence of the first, the 5% significance level is found between 1970 and 1980. Power 1 values are registered in the ≈2, ≈4 and ≈8 year periods and the 5% significance level is obtained in correspondence of the ≈2 year period around 1965. The results concerning phase angle of the analyzed XWT show the in-phase behavior of the selected time series.

The ≈2 and ≈20 year periods of Po river discharge and North Atlantic Oscillation XWT exhibit high power values. This information is also accompanied by the individuation of the 5% significance level that is registered, respectively, in the period 1965-1970 and 1980 and in 1984. The information about phase difference of the two time series is conflicting. Indeed, while in the ≈20 year period Po and NAO are in anti-phase, in the ≈2 year period the arrows point in different directions in different time periods.

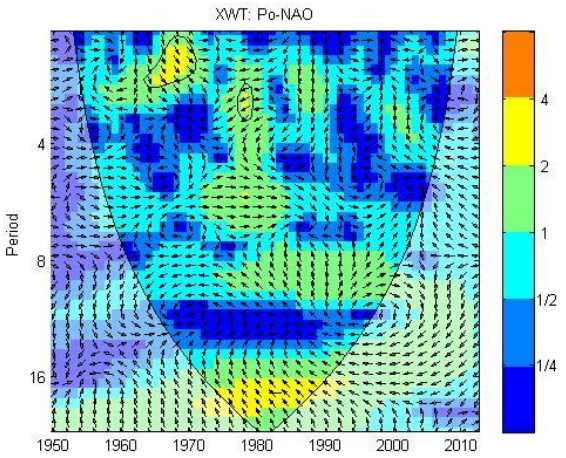

Figure 41: Po and NAO pattern cross wavelet analysis

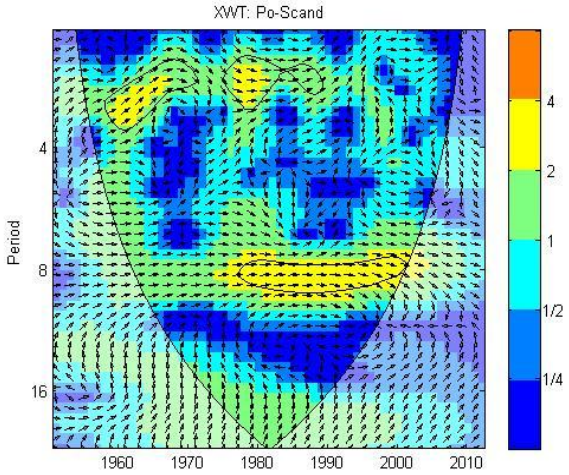

Figure 42: Po and Scandinavia pattern cross wavelet analysis

Figure 42 shows XWT results by analyzing the standardized Po river discharge and the Scandinavia teleconnection pattern time series. High power values are obtained in the ≈2 and ≈8 year periods, while power 1 values are registered in the 2-8 and 16-20 year bands. The 5% significance level is found in correspondence of the ≈2 year period, in the 1960-1970 and 1975-1990 time periods. Moreover, it is observed in the ≈8 year period over a relative long time period between 1980 and 2000. In the areas highlighted by high power values and 5% significance level, the arrows are clearly right-pointing, showing the in-phase behavior of the two considered time series.

The XWT of the standardized Po river discharge and PDO index time series shows high power in the ≈6, ≈8 and ≈20 year periods. The 5% significance level is spotty observed in correspondence of the ≈2 year period around 1940, 1960 and 1980, where wavelet analysis shows power 1. The same significance level is found, the 5% significance level is found in correspondence of the ≈6 year band around 1940, the ≈8 year band between 1990 and 2000 (partly outside the COI) and the ≈20 year period between 1950 and 1970. Most of the results highlighted by high wavelet power and 5% significance show with the right-pointing arrows the in-phase behavior of the analyzed time series.

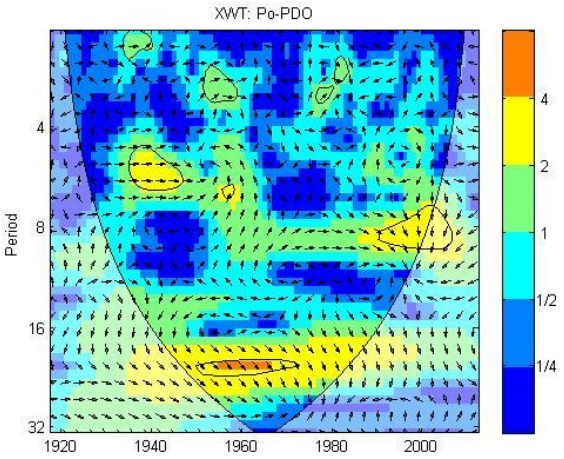

Figure 43: Po and PDO index cross wavelet analysis

6.2.5. Rhone

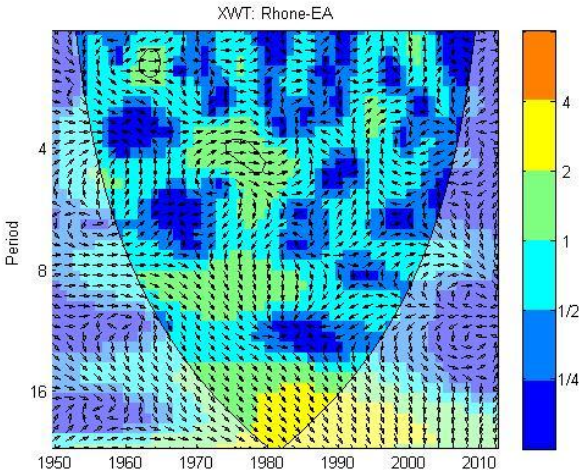

Figure 44: Rhone and EA pattern cross wavelet analysis

Figure 44 shows XWT results by analyzing the standardized Rhone river discharge and the EA teleconnection pattern time series. The highest power values are obtained in the 16-20 year period while power 1 values are registered in the ≈2, ≈4 and ≈8 year periods. The 5% significance level is found in correspondence of the ≈2 year period around 1960 and in correspondence of the ≈4 year period around late 1970s. The results concerning phase angle show the in-phase behavior of the selected time series.

The ≈2 and ≈16 year periods of Rhone river discharge and North Atlantic Oscillation XWT exhibit high power values. This information is also accompanied by the individuation of the 5% significance level that is registered, respectively, around 1965 and in the period between late 1970s and late 1990s. Power 1 signal is found in the 2-6 and ≈8 year bands. The results concerning phase angle in the ≈2 year band do not show a clear behavior of the two time series while in the ≈16 year period the anti-phase behavior of Rhone river discharge and NAO is highlighted by high power values, 5% significance level and left-pointing arrows.

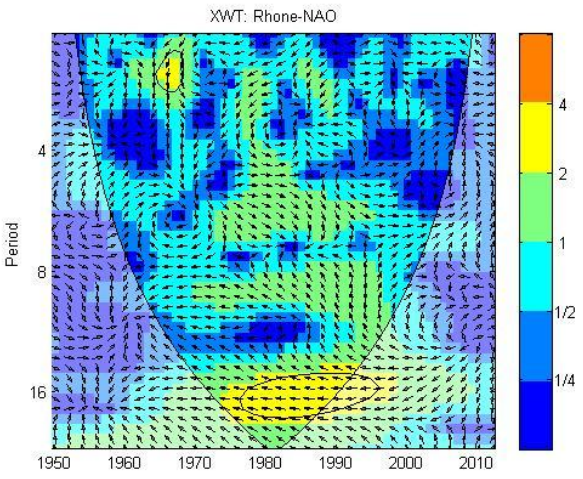

Figure 45: Rhone and NAO pattern cross wavelet analysis

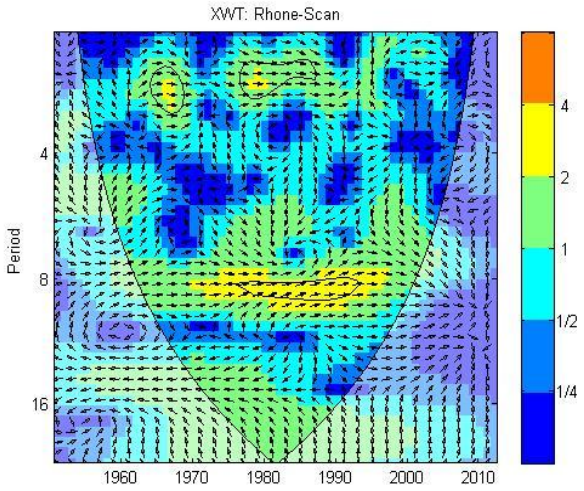

Figure 46: Rhone and Scandinavia pattern cross wavelet analysis

The XWT of the standardized Po river discharge and PDO index time series shows high power in the ≈2 and ≈8 year periods. The 5% significance level is observed in correspondence of the ≈2 year period around 1965, and between 1975 and 1985. The same significance level is found, the 5% significance level is found in correspondence of the ≈8 year band between late 1970s and early 1990s. The results highlighted by high wavelet power and 5% significance show, with the right-pointing arrows, the in-phase behavior of the analyzed time series.

Figure 47 shows XWT results by analyzing the standardized Rhone river discharge and the Pacific Decadal Oscillation index time series High power values are obtained in the 4-6, ≈8 and ≈20 year periods. The 5% significance level is spotty found in correspondence of the ≈2 year period, while in correspondence of the 4-6 year period it covers the time periods 1935-1955 and 1985-1995. Moreover, the significance level is observed in the ≈20 year band around 1960. In most of the observed cases, the arrows point to the right showing the in-phase behavior of the two considered time series.

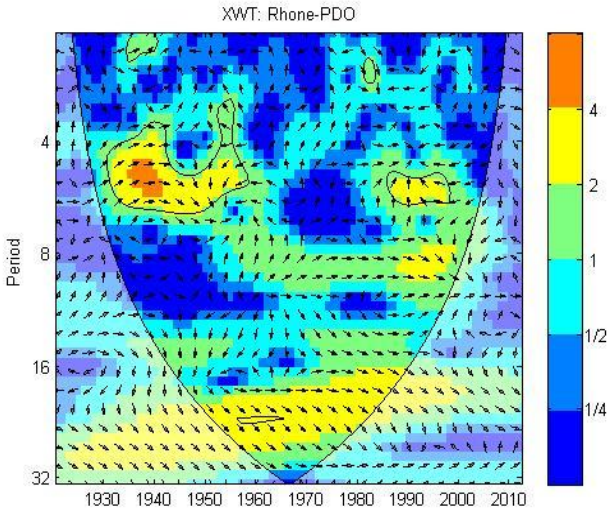

Figure 47: Rhone and PDO index cross wavelet analysis

7. Discussion

This study highlights the effects of variability in atmospheric circulation in determining spatial distribution changes of precipitation, temperature and other climatological elements. The Cross Wavelet Transforms of coupled standardized river discharge and teleconnection patterns time series show how atmospheric variability has an influence on interannual and interdecadal variability of freshwater fluxes that flow from the continents to oceans and seas at different space and time scales. However, it has to be underlined that this type of evaluation is purely qualitative as this study does not allow quantifying the amount of freshwater that is discharged into the Mediterranean Sea.

As discussed in section 2., the five selected rivers contribute to the 70% of the total continental discharge of freshwater into the Mediterranean basin. Thus, the analysis of the selected rivers constitutes a strong basis to evaluate the relation between river discharge and large-scale climate patterns.

This study confirms that wavelet analysis is a useful tool to expand a time series into a time frequency space. The Morlet wavelet maintains a good balance between frequency and time information: for this reason, it can be considered a good choice when using wavelets for feature extraction purposes. By using two CWTs, it is possible to proceed with the XWT that shows its results for the time period covered by the two selected time series. Then, the XWT highlights regions having common power and reveals information about the phase relationship of the analyzed time series (Grinsted et al., 2004).

Significance tests are particularly relevant for the analysis of non-stationary events. The importance of significance test for the wavelet and cross wavelet analysis is justified by the fact that a noise signal can be misinterpreted and confused with a relevant pattern in the wavelet scalogram (Ge, 2007). Thus, the significance tests help in understanding whether the results may have been created by pure casualty or truly have physical meaning. The 5% significance level, obtained through Monte Carlo simulations, has been considered appropriate for the type of study since it has been used for other similar research purposes. The power value that is obtained with wavelet and cross wavelet analyses seems to be relevant to get the 5% significance level: indeed, results show that the outlined significance level is not obtained in correspondence of a certain year period if power value is less than 1. Although certain results show that the 5% significance level is obtained outside the COI, this kind of information maintains anyway its physical meaning and can be object of interpretation.

In this study we exanimate the phase relations between teleconnection patterns and river discharge time series. Phase synchronization is a relationship between phases of two non-stationary signals whose amplitude may be correlated. The interpretation of phase relations is done by analyzing the arrows direction in XWT analyses. Although is known that information related to in-phase and anti-phase behavior of two signals can be highlighted, respectively, by right-pointing and left-pointing arrows, it is still not clear how to interpret the information given by arrows that point in other directions.

The East Atlantic teleconnection pattern shows a behavior that disassociate with the description given in section 3.1.. Indeed, although relevant studies have associated the positive phases of the EA with above-average precipitation over northern Europe and Scandinavia and with below-average precipitation across southern Europe, the obtained results do not confirm this type of observation. The XWT of EA and Adige, Po and Rhone river discharge highlight the in-phase behavior of the analyzed time series. The impact of EA on Ebro and Arno freshwater discharge is less strong, as wavelet power of related XWT does not exceed the 1 value and the information about the 5% significance level within the analyzed time period are not particularly relevant. For River Ebro, possible reasons of this result can be given by the fact that it is the

most regulated river among the ones that are object of this study; while for River Arno a possible explanation could be the relative short time series available related to river discharge data. However, it seems important to underline how the highest cross wavelet power values are found, for all rivers, in correspondence of the same time periods, in particular around the 2-4 and ≈8 year bands.

The North Atlantic Oscillation teleconnection pattern is well known to lead, under positive phases, to above-average precipitation over northern Europe and Scandinavia and to below-average precipitation over southern and central Europe. The NAO index has been also linked, over the 50 past year, with a significant decrease in Mediterranean precipitation (therefore also with a decrease in river discharge) under NAO positive phases (Struglia et al., 2004). This study confirms this observation: the XWTs between NAO and the analyzed rivers show the anti-phase behavior of the time series in the ≈2 and ≈16 year periods. Moreover, the NAO-Po and NAO-Rhone XWTs show similar results, registering common power as well as the 5% significance level in correspondence of the same year bands (i.e. ≈2 and ≈16).

From the CWT of Scandinavia, it is possible to individuate the periodical recurrence of this teleconnections pattern, showing its highest intensity in the ≈2 and ≈8 year period bands. In the same year period bands, the XWTs of Scandinavia teleconnection pattern and selected river discharge time series confirm the thesis that, under positive phases, above-normal precipitations are registered across southern Europe. Indeed, the in-phase behavior of the standardized time series is observed in all the XWTs involving the Scandinavia teleconnection pattern and the rivers' discharge in the ≈2 and ≈8 year periods. This result seems relevant to speculate about the periodical influence of Scandinavia teleconnections pattern on river discharge in the Mediterranean basin. Although the influence on Arno, Po and Rhone rivers is higher, even Adige and Ebro rivers result affected by the periodicity of Scandinavia circulation pattern over the same year period bands (i.e. ≈2 and ≈8).

In regard to the Pacific Decadal Oscillation pattern, many studies have testified its 20-30 years phase variability. For instance, Mantua et al. (2007) have individuated PDO 50-year periodicity with phase persistence of about 25 years. This is also confirmed by the CWT of PDO (see Figure 27) where high wavelet power values are found in correspondence of the 20-30 year period band. Thus, it is not relevant to speculate about PDO influence on climate variability over shorter periods although CWT of PDO shows high wavelet power and 5% significance level also in correspondence of the ≈6 year period band. The XWTs of PDO and the selected river discharge time series show significant result to what concern the relation between the teleconnections pattern and the discharge variability of the rivers. Indeed, the XWTs involving Adige, Po and Rhone rivers show common power and in-phase behavior in correspondence of the 20-30 year period. For the last two rivers, this information is also validated by the 5% significance level (see Figures 43 and 47). Although the XWTs between PDO and Ebro shows less evident results, common power is also found in the 20-30 year period (see Figure 39) while, for River Arno, common power in the 20-30 year period can be only foreseen due to the lack of a longer set of data available (see Figure 31). These results evidence that freshwater discharge variability in the Mediterranean basin is also correlated to PDO fluctuations.

Only a few studies have highlighted the combined effects of the teleconnection patterns on river discharge variability in the Mediterranean area. Zanchettin et al. (2007) have found that, under strong anomalies of NAO, the coupled effects of ENSO and PDO are not relevant while, under weak NAO conditions the coupling of ENSO during positive phases of PDO can be related to wet winter conditions in Europe. Further investigations about the coupling and/or interference of teleconnections patterns can be relevant to clarify their effects on rivers' discharge.

8. Conclusion

In this contribution, it has been examined the relations between continental discharge variability in the Mediterranean basin and four teleconnections patterns. It emerges that the analyzed teleconnection patterns, along with their impact on atmospheric circulation variability, have an influence on annual and decadal variability of freshwater fluxes that flow from the European continent to the sea. However, the relationship between the analyzed non-stationary events is complex.

It is possible to identify three major year bands in which most of the teleconnection patterns are related to river discharge variability in the Mediterranean area. Indeed, the most significant relationships between time series are registered in correspondence of the ≈2, ≈8 and ≈20 year period bands.

The EA pattern mostly influences the northern Rivers that flow into the Mediterranean Sea (i.e. Po and Rhone). These rivers, show an increase of freshwater flux under positive phases of the EA climate pattern. The NAO impacts rivers´ discharge at different time scales. Indeed, it shows its influence on all the selected rivers both over short periods (i.e. around 2 years) and longer ones (i.e. around 20 years) as well as its anti-phase behavior in relation to river discharge variability. The SCA shows a pronounced periodical impact on river discharge variability over the ≈2 and ≈8 year period bands. The analysis carried out from the standardized index series of SCA and the discharge time series of the Mediterranean basin Rivers clearly highlights their in-phase behavior. The PDO impacts the ≈20 year discharge variability of rivers in the Mediterranean area: under its positive phases, this climate pattern seems to be related to an increase of freshwater flow into the Mediterranean Sea.

These potential relations can be useful to predict freshwater discharge variability occurring over the Mediterranean basin. In this regard, further studies are necessary to propose and obtain more robust evaluations. This can be done by broadening this contribution with:

- the analysis of additional rivers that significantly contribute to the freshwater input into the Mediterranean Sea and whose flow is not heavily conditioned by regulatory frameworks;
- the analysis additional climate patterns whose impact is estimated to be relevant within the Mediterranean basin;
- the estimation of the impact of coupling and/or interference between two or more teleconnection patterns;
- the adoption of further statistical methods and as data driven analyses.

Similar studies could lead to a first prediction about future changings in the availability of continental freshwater resources. This could be also useful under a climatic change perspective in relation with possible climate scenarios and evolutions of atmospheric conditions.

9. References

AdB Arno, 2014. **Autorità di Bacino del Fiume Arno: Studi e Documenti**. Online available at http://www.adbarno.it/adb/?page_id=926&biblio=6. Accessed on [31/01/2014].

AdB Po, 2009. **Italian side event "The Po valley compares itself with big international basins".** Online available at http://www.inbo-news.org/IMG/pdf/07_BortoneItaliansideeventfinal.pdf. Accessed on [07/02/2014].

Artioli Y., Bendoricchio G., Palmeri L., 2005. **Defining and modelling the coastal zone affected by the Po river (Italy).** Ecological Modelling, Volume 184 (2005), pages 55–68.

Batalla R.J., Gomez C. M., Kondolf G. M., 2003. **Reservoir-induced hydrological changes in the Ebro River basin (NE Spain).** Journal of Hydrology, Volume 290, pages 117–136.

Barnston A.G. and Livezey R.E. 1987. **Classification, Seasonality and Persistence of Low-Frequency Atmospheric Circulation Patterns**. Monthly Weather Review, Volume 115(6), pp 1083 – 1126.

Bouwer L. M., Vermaat J. E., Jeroen C., 2008. **Regional sensitivities of mean and peak river discharge to climate variability in Europe.** Journal of Geophysical Research, Volume 113, Issue D19.

Bruno M. C., Maiolini B., Silveri L., Carolli M., Kerschbaumer G., 2014. **Alterations of natural flow in field and flume conditions. Conference at the Natural Science Museum of Trento**. Online available at http://www.ecrr.org/archive/conf08/pdf/s8b_6.pdf. Accessed on [07/02/2014]

Cazelles, B., Chavez, M., Berteaux, D., Menard, F., Vik, J.O., Jenouvrier, S., Stenseth, N.C., 2008**. Wavelet analysis of ecological time series**. Oecologia 156, 287–304.

Confederación Hidrográfica del Ebro, 1988. P**lan Hidrológico / Documentación Básica. Technical Report, Zaragoza, 1988.**

Confederacion Hydrografica del Ebro, 2005. **Ebro River Basin Organization**. Online available at http://www.tecniberia.es/jornadas/documentos/Ebro%20River%20Basin.pdf. Accessed on [06/02/2014]

CPC, 2014. **North Atlantic Oscillation (NAO)**. Online available at http://www.cpc.ncep.noaa.gov/data/teledoc/nao.shtml. Accessed on [24/01/2014].

Distretto Idrografico delle Alpi Orientali, 2014. **Piano di gestione dei bacini idrografici delle Alpi Orientali, Bacino del fiume Adige, Capitolo 1, Descrizione generale delle caratteristiche del bacino idrografico dell'Adige.** Online available at http://www.alpiorientali.it/documenti/list_doc/pub/PdP_doc_old/3-documenti_revisionati_al_18_9_2009/PIANO_GESTIONE_COMPLETO_PDF/pg_adige/PG_Adige_1_Corpi_Idrici_rev01.pdf. Accessed on [17/02/2014].

Garcìa, M.A., Moreno, M.C., 2000. **Los aprovechamientos en la Cuenca del Ebro: Afecciòn en el regimen hidrològico fluvial, Internal Technical Report no. 2000-PH-24.1, Confederaciòn Hidrogràfica del Ebro, Zaragoza, 83pp**.

Ge Z., 2007. **Significance tests for the wavelet power and the wavelet power spectrum. Annales Geophysicae, 2007**. Online available at www.ann-geophys.net/25/2259/2007/. Accessed on [18/02/2014]

Grinsted A., Moore J. C., Jevrejeva S., 2004. **Application of the cross wavelet transform and wavelet coherence to geophysical time series.** Nonlinear Processes in Geophysics, 2004. Volume 11, pages 561–566.

Howell P.P., Allan J. A., 1994. **The Nile: Sharing a Scarce Resource: A Historical and Technical Review of water management and of economical and legal issues**. Online available at http://books.google.se/books?id=M_irG57YsWIC&pg=PA141&lpg=PA141&dq=nile+discharge+anthropogenic&source=bl&ots=Rl18n6PJ_P&sig=eo7OoqtaviYF9_Ufs_j-q0miaJs&hl=en&sa=X&ei=3abjUtgiybngBJL_gcgO&ved=0CCUQ6AEwAA#v=onepage&q=nile%20discharge%20anthropogenic&f=false. Accessed on [25/01/2014]

IFC, 2014**. Balkan Renewable Energy Programme (BREP).** Online available at http://www.ifc.org/wps/wcm/connect/region__ext_content/regions/europe+middle+east+and+north+africa/ifc+in+europe+and+central+asia/countries/balkan+renewable+energy+program+(brep). Accessed on [25/01/2014]

IPCC, 2007. **Fourth Assessment Report: Climate Change 2007**. Online available at http://www.ipcc.ch/publications_and_data/ar4/wg1/en/ch3s3-6.html. Accessed on [21/01/2014].

Kawale J., Chatterjeez S., Ormsby D., Steinhaeuser K., Liessy S., Kumar V., 2012. **Testing the Significance of Spatio-temporal Teleconnection Patterns.** Online available at http://www-users.cs.umn.edu/~ksteinha/papers/KDD12.pdf. Accessed [25/01/2014].

Labat D., 2010. **Cross wavelet analyses of annual continental freshwater discharge and selected climate indices.** Journal of Hydrology, Volume 385, Issues 1–4, 7 May 2010, Pages 269–278.

Lidén A. and Olsson K., 2012. **Evaluation of Long-term Discharge in Swedish Rivers**. Examensarbete TVVR 12/5005. Lund University.

Martìn M. L., Luna M. Y., Moratac A., Valero F., 2003. **NORTH ATLANTIC TELECONNECTION PATTERNS OF LOW-FREQUENCY VARIABILITY AND THEIR LINKS WITH SPRINGTIME PRECIPITATION IN THE WESTERN MEDITERRANEAN. INTERNATIONAL JOURNAL OF CLIMATOLOGY**, Vol. 24, pages 213–230 (2004).

Massarutto A., de Carli A., Longhi C., Scarpari M., 2003. **Public Participation in River Basin Management Planning in Italy**. Online available at http://www.harmonicop.uni-osnabrueck.de/_files/_down/Italy.pdf. Accessed on [11/02/2014].

MIMAM, 2000. **Ministerio de Medio Ambiente, Libro Blanco del Agua en Espana. Chapter 3, La situacion actual y los problemas existents y previsibles.**

Muñoz I., Prat N., 1989. **Effects of river regulation on the lower Ebro river (NE Spain).** River Research and Application, Volume 3, Issue 1, pages 345–354, January/April 1989.

North Carolina Climate Office, 2014. Online available at http://www.nc-climate.ncsu.edu/climate/patterns/PDO.html. Accessed [24/01/2014].

Provincia di Firenze, 2012. **Energia idroelettica dall'Arno.** Online available at http://www.provincia.fi.it/ambiente/arno/energia-idroelettrica-dallarno/. Accessed on [31/01/2014].

Regione Toscana, 2014. **Bacino del Fiume Arno - Parte A - Quadro di riferimento conoscitivo e programmatico.** Online available at http://www.regione.toscana.it/documents/10180/70262/Piano%20tutela%20acque%20Arno%20cap%201,2,3_64022/73ad8bf1-8e86-42c7-a51d-36ecc1a05d03. Accessed on [31/01/2014].

Souchon Y., 2004. **The Rhone river: hydromorphological and ecological rehabilitation of a heavily man-used hydrosystem.** Assessment and Provision of Environmental Flows in Mediterranean Watercourses - Basic Concepts, Methodologies and Emerging Practice. Online available at http://cmsdata.iucn.org/downloads/france.pdf. Accessed on [03/02/2014].

Struglia M.V., Mariotti A., Filograsso A., 2004. **River discharge into the Mediterranea Sea: Climatology and aspects of the observed variability**. Journal of Climate, Volume 17, pages 4740-4751.

W2A, 2014. **Resilience enhancement and water demand management for climate change adaptation.** Online available at http://www.feem-project.net/water2adapt/01_project_02.html. . Accessed on [07/02/2014]

Zanchettin, D. ; Franks, S. W. ; Traverso, P. ; Tomasino, M., 2007. **On ENSO impacts on European wintertime rainfalls and their modulation by the NAO and the Pacific multi-decadal variability described through the PDO index.** INTERNATIONAL JOURNAL OF CLIMATOLOGY, Volume 28, pages 995-1006

10. Figures References

Figure 1. Struglia M.V., Mariotti A., Filograsso A., 2004. River discharge into the Mediterranea Sea: Climatology and aspects of the observed variability. Journal of Climate, Volume 17, pages 4740-4751.

Figure 2. Weather Almanac, 2014. Online available at http://www.islandnet.com/~see/weather/almanac/arc2007/alm07mar.htm. Accessed on [17/02/2014]

Figure 3. Autorità di Bacino del Fiume Adige, 2014. Online available at http://213.21.149.34:2725/monitoraggi/dati_online.php. Accessed on [07/02/2014]

Figure 4. Autorità di Bacino del Fiume Arno, 2014. Online available at http://www.adbarno.it/adb/. Accessed on [08/02/2014]

Figure 5. Wikimedia Commons, 2007. Online available at http://commons.wikimedia.org/wiki/File:SpainEbroBasin.png. Accessed on [09/02/2014]

Figure 6. Wikipedia, 2008. Online available at http://en.wikipedia.org/wiki/File:Po_bacino_idrografico.png. Accessed on [09/02/2014]

Figure 7. Souchon Y., 2004. The Rhone river: hydromorphological and ecological rehabilitation of a heavily man-used hydrosystem. Assessment and Provision of Environmental Flows in Mediterranean Watercourses - Basic Concepts, Methodologies and Emerging Practice. Online available at http://cmsdata.iucn.org/downloads/france.pdf. Accessed on [03/02/2014].

Figure 8. Engström J., 2011. Impacts of Northern Hemisphere teleconnections on the hydropower production in southern Sweden. Department of Earth and Ecosystem Sciences, Physical Geography and Ecosystems Analysis, Lund University. Available at:

http://lup.lub.lu.se/luur/download?func=downloadFile&recordOId=2438792&fileOId=2438794. Accessed on [26/01/2014]

Figure 9. CPC, 2014a. Online available at http://www.cpc.ncep.noaa.gov/data/teledoc/ea_ts.shtml. Accessed on [27/01/2014]

Figure 10. CPC, 2014b. Online available at http://www.cpc.ncep.noaa.gov/data/teledoc/nao_ts.shtml. Accessed on [27/01/2014]

Figure 11 and 12. Bell I., 2009. North Atlantic Oscillation, Positive NAO Index and Negative NAO index. Online Available at: <http://www.ldeo.columbia.edu/res/pi/NAO/>, [Accessed on 25/01/2014]

Figure 13. CPC, 2014b. Online available at http://www.cpc.ncep.noaa.gov/data/teledoc/scand_ts.shtml. Accessed on [27/01/2014]

Figure 14. Climate Impact Group, University of Washington, 2014. Online available at http://cses.washington.edu/cig/figures/pdoensoglobe_BIG.gif. Accessed on [28/02/2014]

Figure 15. Tokyo Climate Center, 2014. Online available at http://ds.data.jma.go.jp/tcc/tcc/products/elnino/decadal/pdo_month.html. Accessed on [30/01/2014]

Figure 16. Torrence C. and Compo G.P., 1998. A Practical Guide to Wavelet Analysis. Bulletin of the American Meteorological Society.

Figure 17. Lidén A. and Olsson K., 2012. Evaluation of Long-term Discharge in Swedish Rivers. Examensarbete TVVR 12/5005. Lund University.

Appendix 1. Matlab codes

Performing wavelet and cross wavelet analyses

```
% This example illustrates how to perform
% continuous wavelet transform (CWT), Cross wavelet transform (XWT)
% and Wavelet Coherence (WTC) plots of your own data.

% Modified by CBU
% http://www.pol.ac.uk/home/research/waveletcoherence/

%% Load the data
% First we load the two time series into the matrices d1 and d2.

seriesname={'river'; 'teleconnectionpattern'};
load teleconnectionpattern.mat
d1=river (1:end,:);
d2=teleconnectionpattern(1:end,:);
%  seriesname={'Arno' 'EA'}
%  d1=load('arno_2012.txt');
%  d2=load('eapattern.txt');

%% Continuous wavelet transform (CWT)
% The CWT expands the time series into time-frequency space
& The result is two figures showing CWTs of river discharge and teleconnections
pattern time series

figure('color',[1 1 1])
opengl software
tlim=[min(d1(1,1),d2(1,1)) max(d1(end,1),d2(end,1))];
subplot(2,1,1);
wt_cin(d1);
title('river');
set(gca,'xlim',tlim);
subplot(2,1,2)
wt_cin(d2)
title('teleconnectiopattern')
set(gca,'xlim',tlim)

%% Cross wavelet transform (XWT)
% The XWT finds regions in time frequency space where the time series show high
common power.
% The result is one figure showing common power, significance level and phase
angle
figure('color',[1 1 1])
opengl software
xwt_cin(d1,d2)
title(['XWT: river-teleconnectionpattern'])

%% Copyright notice
%   Copyright (C) 2002-2004, Aslak Grinsted
%   This software may be used, copied, or redistributed as long as it is not
%   sold and this copyright notice is reproduced on each copy made.  This
%   routine is provided as is without any express or implied warranties
%   whatsoever.
```